Eddy-current asymptotics of the Maxwell PMCHWT formulation for multiple bodies and conductivity levels

Marc Bonnet, Edouard Demaldent

EDDY-CURRENT ASYMPTOTICS OF THE MAXWELL PMCHWT FORMULATION FOR MULTIPLE BODIES AND CONDUCTIVITY LEVELS

MARC BONNET[1] AND EDOUARD DEMALDENT[2]

ABSTRACT. In eddy current (EC) testing applications, ECs $\sigma\boldsymbol{E}$ ($\boldsymbol{E}$: electric field, σ: conductivity) are induced in tested metal parts by a low-frequency (LF) source idealized as a closed current loop in air. In the case of highly conducting (HC) parts, a boundary integral equation (BIE) of the first kind under the magneto-quasi-static approximation - which neglects the displacement current - was shown in a previous work to coincide with the leading order of an asymptotic expansion of the Maxwell BIE in a small parameter reflecting both LF and HC assumptions. The main goal of this work is to generalize the latter approach by establishing a unified asymptotic framework that is applicable to configurations that may involve multiple moderately-conducting ($\sigma = O(1)$) and non-conducting objects in addition to (possibly multiply-connected) HC objects. Leading-order approximations of the quantities relevant to EC testing, in particular the impedance variation, are then found to be computable from a reduced set of primary unknowns (three on HC objects and two on other objects, instead of four per object for the Maxwell problem). Moreover, when applied to the Maxwell BIE, the scalings suggested by the asymptotic approach stabilize the condition number at low frequencies and remove the low-frequency breakdown effect. The established asymptotic properties are confirmed on 3D numerical examples for simple geometries as well as two EC testing configurations, namely a classical benchmark and a steam generator tube featured in pressurized water reactors of nuclear power plants.

Eddy currents, defined by $\sigma\boldsymbol{E}$ (where $\boldsymbol{E}$ is the electric field and σ the medium conductivity), arise in various areas of industry, in connection with e.g. braking of heavy vehicles, heating processes using induction, or nondestructive evaluation by eddy current testing (ECT), the latter application being the main practical motivation behind this work. In ECT procedures [33], currents are induced in the metallic body undergoing inspection by a low-frequency source idealized as a closed loop of electric current in air (by contrast with capacitive applications associated with open loops). The main observable quantities of interest are the impedance variation at the coil terminals and the magnetic field $\boldsymbol{H}$, while the simulation of ECT experiments also serves to quantify the currents $\sigma\boldsymbol{E}$ in the inspected region. The EC model is the magneto-quasistatic approximation of the Maxwell transmission problem where the displacement currents $\varepsilon_{\rm diel}\boldsymbol{E}$ (with $\varepsilon_{\rm diel}$ the electric permittivity of the medium) are negligible. This approximation is relevant in ECT experiments, as they usually involve highly conducting objects and low operating frequencies, so that the EC model can be considered as a limiting form of the Maxwell model.

These considerations prompted us to introduce in [6] the dimensionless parameter $\gamma := \sqrt{\omega\varepsilon_0/\sigma}$, which, combined with specifying the operating skin depth, reflects ECT conditions in the limit $\gamma \to 0$, and derive the small-γ asymptotic expansion of the PMCHWT integral equation formulation [25] for the electromagnetic transmission problem for a highly conducting body surrounded by vacuum. In particular, we rigorously proved that the resulting integral equation system governing the leading-order contribution to the surface currents is the same as that, established in [18], governing the EC problem. Among its advantages, this limiting formulation allows to obtain the leading-order approximations of the magnetic field in $\mathbb{R}^3$, the eddy currents in the conducting bodies and the impedance variations from the solution of a boundary integral equation (BIE) system governing three unknown scalar functions, instead of the four (two components for each tangential current density) involved in the original PMCHWT problem; an additional post-processing is necessary if one also needs $\boldsymbol{E}$ in the surrounding non-conducting medium. In addition to finding limiting problems with reduced numbers of unknowns, treating the transmission problem as dependent on γ allows to obtain insight and develop computational formulations achieving a

[1]POEMS, ENSTA PARIS, 91120 PALAISEAU, FRANCE
[2]UNIVERSITÉ PARIS-SACLAY, CEA, LIST, F-91120, PALAISEAU, FRANCE
E-mail addresses: mbonnet@ensta.fr,edouard.demaldent@cea.fr.
Date: March 25, 2023.

transition from the full Maxwell equation system to the EC model, and to extend EC-type approximations to mid-frequency testing for complex media (e.g. made of fibers with diverse conductivities). The main goal of this work is accordingly to extend the expansion approach of [6] to configurations that involve multiple objects that may be highly conducting (HC), moderately-conducting (MC) or non-conducting (NC).

The PMCHWT formulation is a first-kind system of integral equations that is known to suffer from the so-called low-frequency breakdown [10]. This phenomenon, which creates dominant numerical noise at low frequencies, results from the antagonist asymptotic behaviors of the charge-carrying and charge-free current densities in the dielectric single layer potential. Applying a Helmholtz-Hodge decomposition to the approximation space allows to dissociate these competing contributions; this is in practice done by working with H_{div}-conforming boundary element (BE) approximations and defining a subspace of charge-free linear combinations of basis functions and its supplementary subspace [1] (an approach often known as the loop-tree or loop-star decomposition). This played in particular an important role in the asymptotic analysis of [6], by separately rescaling the loop and tree components of the surface unknowns. As a result, unlike in the original PMCHWT formulation, the condition number of the resulting rescaled Maxwell BE system is stable in the low-frequency limit, albeit not low enough for iterative solvers; moreover, constructing all the loop basis functions may entail significant computational work on large models involving multiply-connected bodies. A recent BIE formulation for the Maxwell problem suitable for modeling the low-frequency inspection of conducting objects [11], based on a rescaled and preconditioned version of the PMCHWT problem, remedies both issues; this formulation however retains four unknown functions. Moreover, the preconditioning approach prevents the removal of certain double-layer operators that are known to identically vanish while causing numerical noise if kept in the BE discretization process.

As an alternative to the Helmholtz decomposition, the low frequency breakdown can be circumvented by introducing a scalar unknown which ensures the relation between the current and the charge according to the formula $\boldsymbol{u}\cdot\boldsymbol{n}|_S = \kappa^{-2}\mathrm{div}_S\big(\mathbf{rot}\,\boldsymbol{u}\times\boldsymbol{n}|_S\big)$ where $\boldsymbol{n}$ and κ correspond to the normal and the wave number in the medium on either side of the relevant surface S. In practice, the normal component $\boldsymbol{E}\cdot\boldsymbol{n}$ which carries the electric charge is then considered identically zero in the magneto-quasistatic form. A magneto-quasistatic second-kind BIE for the vector unknown $\boldsymbol{J} = \boldsymbol{n}\times\boldsymbol{H}$ (2 scalar tangential components) and the scalar unknown $m := \mu\boldsymbol{H}\cdot\boldsymbol{n}$ was proposed in [23] and studied in [19]. Several follow-up contributions, e.g. [20], then aimed at improving solution accuracy near sharp edges. For piecewise-planar surfaces, this issue is essentially the same as that of accurately computing near-field double-layer influence terms, see e.g. [21, 22]. In particular, surface currents $\boldsymbol{J} = \boldsymbol{n}\times\boldsymbol{H}$ are represented in [28] with three scalar components in $H^{1/2}(\Gamma)$ (so $\boldsymbol{J}$ is no longer merely H_{div}-regular, while the BIE system has four scalar unknowns), to enforce continuous approximations of surface currents and improve solution stability at the sharp edges; this formulation has to our knowledge been developed for non-ECT applications. Another magneto-quasistatic second-kind BIE, involving two unknown tangential vector fields and one scalar unknown (i.e. five scalar unknowns on the surface of a highly conducting object) has been proposed in [35, 4], this time for ECT simulations. Another recently-proposed BIE formulation for Maxwell problems [29], based on potentials instead of fields, is numerically demonstrated to behave well over large ranges of skin depths that include ECT conditions, albeit at the inherent expense of larger sets of surface unknowns.

A HLU preconditioner (resulting from the factorization of the linear system produced by $\mathcal{H}$-matrix compression and ACA) for the BIE formulation of [28] is studied in [30], while an iterative solver for the BIE of [4] accelerated by $\mathcal{H}$-matrix compression and ACA or truncated and degenerated kernel function method was recently proposed in [3] and [5], respectively. Such developments make iterative methods for large-scale ECT models feasible. Alternatively, in view of the spatially-localized nature of the source and the quasistatic regime inherent to ECT, gradually coarser discretizations may usually be adopted away from the vicinity of the sensor. This, and keeping the number of unknown scalar functions to a minimum, allows the simulation of complete EC scans of inspected zones using direct solvers. Our work adopts this philosophy, and first-kind BIE formulations such as those used in [18] and [6], featuring reduced sets of unknowns, appear best suited to it.

Accordingly, extending our previous investigation [6] (where only HC objects were considered), we scale low frequencies and large conductivities of HC bodies in terms of a small parameter η, whose definition

differs from γ introduced in [6] in order to treat configurations that may involve highly conducting (HC), moderately-conducting (MC) and non-conducting (NC) objects in a unified asymptotic framework. We then derive the small-η asymptotic expansion of the first-kind PMCHWT integral equation system for configurations comprising arbitrary numbers of HC, MC and NC objects (whereas only HC objects were considered in [6]), in such a way that the remainder of each obtained expansion in each medium is of order $O(\eta^2)$ relative to the leading-order term. The resulting asymptotic approximations becomes equivalent to the small-γ expansion of [6] for configurations involving just a HC body in air, for which that same order of approximation was shown to be achieved by the leading-order contribution. Here, the presence of MC objects is shown to introduce, within the chosen expansion order, additional terms beyond the leading order that otherwise would vanish. We also extend the asymptotic formulation of [6] to accommodate bi-material objects involving differing conductivity levels (e.g. a HC core embedded in a MC or NC material) and multiply-connected objects. To focus on providing a unified asymptotic approach for configurations involving diverse classes of conductivity and its practical merits and implications, and also to avoid excessive length, the asymptotic derivation is here conducted formally, forgoing the rigorous justification of the truncation error order. Such justification was given in [6] for a HC body in vacuum, and we expect the main arguments used there to extend to the present framework.

The obtained asymptotic approximation of the PMCHWT problem is useful on several counts. Firstly, leading-order approximations of the relevant quantities are found to be computable from the solution of integral problems involving reduced sets of unknowns (namely three on HC objects and two on other objects) and based on simpler integral operators, yielding several-fold reduction of computational work (relative to the Maxwell PMCHWT system with the same BE mesh) under conditions typical of ECT. Then, the obtained expansions imply that achievable approximation orders vary depending on whether MC bodies are involved. Those expansions also show how to obtain the optimal accuracy achievable by leading-order approximations with the least amount of computation. Finally, applying to the Maxwell PMCHWT problem the scalings suggested by the asymptotic approach stabilizes the condition number at low frequencies and removes the low-frequency breakdown effect.

This article is organized as follows. Our starting point is the well-known PMCHWT integral formulation for the electromagnetic transmission problem [25] with a Hodge decomposition applied to the unknown surface currents, which is recalled in Sec. 1. Then, we introduce in Section 2 the parameter η into the PMCHWT problem, derive the problems governing the first three coefficients of the solution expansion in η, and obtain resulting expansions for the electromagnetic fields and impedance variation. Special cases and extensions are considered in Section 3, in particular bi-material or multiply-connected objects. Finally, a boundary element (BE) method for the PMCHWT problem, incorporating a Hodge decomposition, is concisely described in Sec. 4, and the established asymptotic properties are demonstrated on 3D numerical examples for simple geometries as well as two ECT configurations. Regarding the latter, one is a classical ECT benchmark for which we obtain an impedance curve comparable to the reference data with a BE system of only a few thousand unknowns, and the other models the inspection of steam generator tubes in pressurized water reactors of nuclear power plants. The BE formalism underpinning this work has in fact been used, with the French national institute expert in safety and radioprotection (IRSN), for technical studies on such tubes [16, 17, 31], and a dedicated module is now available in the simulation platform CIVA [12].

1 Maxwell transmission problem and PMCHWT integral formulation.

1.1 Configuration and governing equations. We assume time-harmonic conditions with given angular frequency ω. We consider the transmission problem whereby M three-dimensional bounded conducting objects with complex permittivities $\varepsilon_a = \varepsilon_0\varepsilon_{ra}^{\mathrm{d}} + \mathrm{i}\sigma_a/\omega$ and permeabilities $\mu_a = \mu_0\mu_{ra}$ $(1 \le a \le M)$, which occupy the bounded Lipschitz domains $\Omega_a \subset \mathbb{R}^3$, are surrounded by vacuum (with permittivity ε_0 and permeability μ_0) filling the connected unbounded complement $\Omega_0 := \mathbb{R}^3 \setminus (\overline{\Omega_1} \cup \ldots \cup \overline{\Omega_M})$ (Fig. 1). The objects are disjoint (I.E. $\overline{\Omega_a} \cap \overline{\Omega_b} = \emptyset$, $1 \le a < b \le M$) and the unit normal $\boldsymbol{n}$ on each object boundary $\Gamma_a = \partial\Omega_a$ points into Ω_0 (i.e. is exterior to Ω_a). We assume for now that each object is homogeneous and each Γ_a is simply connected (extensions to bi-material and multiply-connected objects being treated in Sections 3.3 and 3.4). The objects are excited by electric and magnetic fields, which are created by a given current density $\boldsymbol{J}_{\mathrm{s}}$ assumed to have a compact support $D \Subset \Omega_0$ and solve Maxwell's equations in

vacuum outside of D. As a result of the foregoing assumptions, the electric and magnetic fields $\boldsymbol{E}$ and $\boldsymbol{H}$ solve the linear frequency-domain Maxwell equations

$$\begin{aligned} &\mathbf{rot}\,\boldsymbol{E} = \mathrm{i}\omega\mu_0\boldsymbol{H}, \qquad \mathbf{rot}\,\boldsymbol{H} = -\mathrm{i}\omega\varepsilon_0\boldsymbol{E} + \boldsymbol{J}_\mathrm{s} && \text{in } \Omega_0,\\ &\mathbf{rot}\,\boldsymbol{E} = \mathrm{i}\omega\mu_a\boldsymbol{H}, \qquad \mathbf{rot}\,\boldsymbol{H} = -\mathrm{i}\omega\varepsilon_0\varepsilon_{\mathrm{r}a}^{\mathrm{d}}\boldsymbol{E} - \sigma_a\boldsymbol{E} && \text{in } \Omega_a,\ 1\le a\le M. \end{aligned}$$

In addition, $\boldsymbol{E}$ and $\boldsymbol{H}$ in Ω_0 are assumed to satisfy the Silver-Müller radiation condition at infinity:

$$\left|\mathbf{rot}\,\boldsymbol{u}\times\frac{\boldsymbol{r}}{|\boldsymbol{r}|} - \mathrm{i}\omega\sqrt{\varepsilon_0\mu_0}\boldsymbol{u}\right| = O(|\boldsymbol{r}|^{-1}), \quad |\boldsymbol{r}|\to\infty \qquad (\boldsymbol{u}=\boldsymbol{E},\boldsymbol{H}). \tag{1}$$

Adopting $\boldsymbol{E}$ as the primary unknown, the above-described problem hence gives rise to the following transmission problem for the electric fields $\boldsymbol{E}_0$ in the vacuum Ω_0 and $\boldsymbol{E}_a$ in each object Ω_a:

$$\begin{aligned} &(\mathbf{rot}\,\mathbf{rot}\, - \kappa_0^2)\boldsymbol{E}_0 = \mathrm{i}\omega\mu_0\boldsymbol{J}_\mathrm{s} && \text{in } \Omega_0, && \boldsymbol{\gamma}_\times^{a-}\boldsymbol{E}_a - \boldsymbol{\gamma}_\times^{a+}\boldsymbol{E}_0 = \boldsymbol{0} && \text{on } \Gamma_a,\\ &(\mathbf{rot}\,\mathbf{rot}\, - \kappa_a^2)\boldsymbol{E}_a = \boldsymbol{0} && \text{in } \Omega_a, && \mu_{\mathrm{r}a}^{-1}\boldsymbol{\gamma}_N^{a-}\boldsymbol{E}_a - \boldsymbol{\gamma}_N^{a+}\boldsymbol{E}_0 = \boldsymbol{0} && \text{on } \Gamma_a, \quad 1\le a\le M,\\ & && \boldsymbol{E}_0 \text{ satisfies (1)} && && \text{at infinity,} \end{aligned} \tag{2}$$

wherein $\mathbf{rot}$ stands for the curl operator, the wavenumbers κ_0 in the vacuum and κ_a in each body Ω_a are given by

$$\kappa_0^2 = \varepsilon_0\mu_0\omega^2, \qquad \kappa_a^2 = \kappa_0^2\big(\varepsilon_{\mathrm{r}a}^{\mathrm{d}} + \mathrm{i}\frac{\sigma_a}{\omega\varepsilon_0}\big)\mu_{\mathrm{r}a}, \qquad 1\le a\le M,$$

and the boundary trace operators $\boldsymbol{\gamma}_\times^{a\pm}$, $\boldsymbol{\gamma}_N^{a\pm}$ acting on vector fields are defined by

$$\boldsymbol{\gamma}_\times^{a\pm}\boldsymbol{u} := \boldsymbol{\gamma}^{a\pm}\boldsymbol{u}\times\boldsymbol{n}, \quad \boldsymbol{\gamma}_N^{a\pm}\boldsymbol{u} := \boldsymbol{\gamma}_\times^{a\pm}\mathbf{rot}\,\boldsymbol{u} \quad (1\le a\le M) \tag{3}$$

where $\boldsymbol{\gamma}^{a+}\boldsymbol{u}$ and $\boldsymbol{\gamma}^{a-}\boldsymbol{u}$ are the exterior and interior Dirichlet traces of $\boldsymbol{u}$ on Γ_a, i.e. (for sufficiently regular fields $\boldsymbol{u}$) the values on Γ_a of $\boldsymbol{u}|_{\overline{\Omega_0}}$ and $\boldsymbol{u}|_{\overline{\Omega_a}}$.

Incident field. Let $G(\cdot;\kappa)$ be the fundamental solution of $-(\Delta+\kappa^2)G = \delta$ for a medium characterized with the wavenumber κ, given by

$$G(\boldsymbol{z};\kappa) = \frac{e^{\mathrm{i}\kappa|\boldsymbol{z}|}}{4\pi|\boldsymbol{z}|}, \qquad \boldsymbol{z}\in\mathbb{R}^3\setminus\{\boldsymbol{0}\}.$$

Let the incident electric field created in the vacuum medium by the given current density $\boldsymbol{J}_\mathrm{s}$ be given by the Biot-Savart law, i.e.

$$\boldsymbol{E}^{\mathrm{inc}}(\boldsymbol{x}) = \mathrm{i}\omega\mu_0\boldsymbol{\Phi}[\boldsymbol{J}_\mathrm{s}], \tag{4}$$

where $\boldsymbol{\Phi}[\boldsymbol{J}]$ is the volume potential (with density $\boldsymbol{J}$ of support D) in the vacuum medium, defined by

$$\boldsymbol{\Phi}[\boldsymbol{J}] := \int_D G(\boldsymbol{x}-\boldsymbol{x}';\kappa_0)\boldsymbol{J}(\boldsymbol{x}')\,\mathrm{d}V(\boldsymbol{x}'). \tag{5}$$

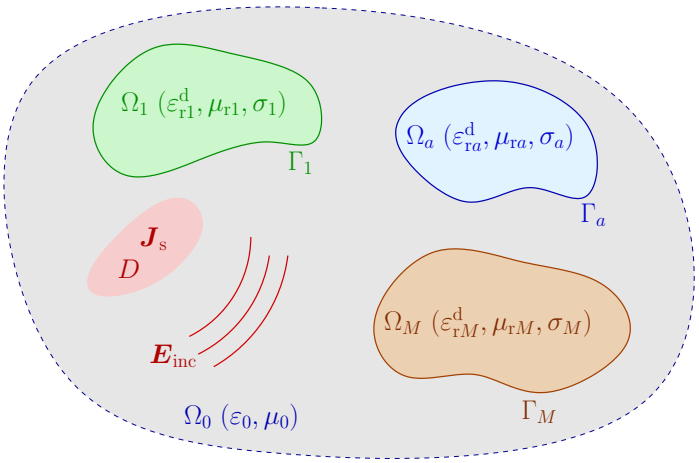

Figure 1. *Scattering by multiple objects: geometry and notation.*

In problem (2), $\boldsymbol{J}_{\rm s}$ is assumed to satisfy

$$\operatorname{div}\boldsymbol{J}_{\rm s}=0 \quad \text{in } D, \qquad \boldsymbol{J}_{\rm s}\cdot\boldsymbol{n}=0 \quad \text{on } \partial D, \tag{6}$$

in which case the incident electric field (4) satisfies $(\mathbf{rot}\,\mathbf{rot}\,-\kappa_0^2)\boldsymbol{E}^{\rm inc}=\mathrm{i}\omega\mu_0\boldsymbol{J}_{\rm s}$ in $\mathbb{R}^3$ and the radiation condition (1). For a torus-shaped bobbin coil of cross-section area s_c, composed of n_c turns and for an injected current I, $\boldsymbol{J}_{\rm s}$ is given by

$$\boldsymbol{J}_{\rm s}=I\hat{\boldsymbol{J}}_{\rm s} \qquad \text{with} \quad \hat{\boldsymbol{J}}_{\rm s}=\frac{n_c}{s_c}\boldsymbol{\tau} \tag{7}$$

in terms of n_c, s_c and the unit tangent vector $\boldsymbol{\tau}$ to the central line of the torus, and verifies (6).

1.2 Stratton-Chu integral representation formulas.

The integral formulation of the electromagnetic transmission problem uses surface potentials created by tangential current densities on the surfaces Γ_a. The latter may be assumed to belong to spaces of tangential vector fields $\boldsymbol{\mathcal{V}}^a$ defined by

$$\boldsymbol{\mathcal{V}}^a := \big\{\, \boldsymbol{v}\in \boldsymbol{H}_{\parallel}^{-1/2}(\Gamma_a) :\ \operatorname{div}_S\boldsymbol{v}\in H^{-1/2}(\Gamma_a)\,\big\},$$

where $\boldsymbol{H}_{\parallel}^{-1/2}(\Gamma_a)$ is the $L^2(\Gamma_a;\mathbb{R}^3)$ dual of $\boldsymbol{H}_{\parallel}^{1/2}(\Gamma):=\boldsymbol{n}\times\big(\boldsymbol{\gamma}^{a-}H^1(\Omega_a;\mathbb{R}^3)\times\boldsymbol{n}\big)$ and div_S denotes the surface divergence operator, see e.g. [24, Sec. 2.5.6].

Let the single-layer Helmholtz potential generated by a tangential current density $\boldsymbol{u}\in\boldsymbol{\mathcal{V}}^a$ be given by

$$\boldsymbol{\mathcal{A}}_\ell^a[\boldsymbol{u}](\boldsymbol{x}) := \int_{\Gamma_a} G(\boldsymbol{x}-\boldsymbol{x}';\kappa_\ell)\boldsymbol{u}(\boldsymbol{x}')\,\mathrm{d}S(\boldsymbol{x}') \qquad (\ell=0,\dots,M;\ a=1,\dots,M).$$

Then, the single- and double-layer Maxwell potentials $\boldsymbol{\mathcal{S}}_\ell^a, \boldsymbol{\mathcal{D}}_\ell^a$ are defined in terms of $\boldsymbol{\mathcal{A}}_\ell^a$ by

$$\begin{aligned} &\boldsymbol{\mathcal{S}}_\ell^a[\boldsymbol{u}]=\boldsymbol{\mathcal{A}}_\ell^a[\boldsymbol{u}]+(\kappa_\ell L)^{-2}\boldsymbol{\mathcal{K}}_\ell^a[\boldsymbol{u}] \quad (\kappa_\ell\neq 0), \qquad \boldsymbol{\mathcal{K}}_\ell^a[\boldsymbol{u}]:=L^2\boldsymbol{\nabla}\boldsymbol{\mathcal{A}}_\ell^a[\operatorname{div}_S\boldsymbol{u}],\\ &\boldsymbol{\mathcal{D}}_\ell^a[\boldsymbol{u}]=L\mathbf{rot}\,\boldsymbol{\mathcal{A}}_\ell^a[\boldsymbol{u}], \end{aligned} \tag{8}$$

where L is a characteristic length (such as a representative body diameter) allowing all potentials to have the same units. They are Maxwell solutions in $\mathbb{R}^3\setminus\Gamma_a$ (for the wavenumber κ_ℓ), verify the interrelations

$$L\mathbf{rot}\,\boldsymbol{\mathcal{S}}_\ell^a=\boldsymbol{\mathcal{D}}_\ell^a, \qquad L\mathbf{rot}\,\boldsymbol{\mathcal{D}}_\ell^a=(\kappa_\ell L)^2\boldsymbol{\mathcal{S}}_\ell^a, \tag{9}$$

and define continuous $\boldsymbol{\mathcal{V}}^a\to\boldsymbol{H}(\mathbf{rot}\,\mathbf{rot}\,,\Omega_a)$ and $\boldsymbol{\mathcal{V}}^a\to\boldsymbol{H}_{\rm loc}(\mathbf{rot}\,\mathbf{rot}\,,\mathbb{R}^3\setminus\overline{\Omega_a})$ linear operators [9], where

$$\begin{aligned} \boldsymbol{H}_{\rm loc}(\mathbf{rot}\,\mathbf{rot}\,,\Omega)&=\big\{\,\boldsymbol{u}\in L^2_{\rm loc}(\Omega;\mathbb{R}^3):\ \mathbf{rot}\,\mathbf{rot}\,\boldsymbol{u}\in L^2_{\rm loc}(\Omega;\mathbb{R}^3)\,\big\},\\ \boldsymbol{H}(\mathbf{rot}\,\mathbf{rot}\,,\Omega)&=\big\{\,\boldsymbol{u}\in L^2(\Omega;\mathbb{R}^3):\ \mathbf{rot}\,\mathbf{rot}\,\boldsymbol{u}\in L^2(\Omega;\mathbb{R}^3)\,\big\} \end{aligned}$$

Using these definitions, the well-known Stratton-Chu integral representation formula for the electric field (see e.g. [13, Thm. 6.2]) reads

$$\boldsymbol{E}_0=\boldsymbol{E}^{\rm inc}-\sum_{a=1}^M\big(\boldsymbol{\mathcal{S}}_0^a[\boldsymbol{\gamma}_N^{a+}\boldsymbol{E}]+\boldsymbol{\mathcal{D}}_0^a[L^{-1}\boldsymbol{\gamma}_\times^{a+}\boldsymbol{E}]\big) \quad \text{in } \Omega_0, \qquad \boldsymbol{E}_a=\boldsymbol{\mathcal{S}}_a^a[\boldsymbol{\gamma}_N^{a-}\boldsymbol{E}]+\boldsymbol{\mathcal{D}}_a^a[L^{-1}\boldsymbol{\gamma}_\times^{a-}\boldsymbol{E}] \quad \text{in } \Omega_a$$

Then, defining on each Γ_a the surface current densities $\boldsymbol{J}^a, \boldsymbol{M}^a$ given by

$$\boldsymbol{\gamma}_N^{a+}\boldsymbol{E}_0=\mathrm{i}\omega\mu_0\boldsymbol{J}^a, \qquad \boldsymbol{\gamma}_N^{a-}\boldsymbol{E}_a=\mathrm{i}\omega\mu_0\mu_{{\rm r}a}\boldsymbol{J}^a, \qquad \boldsymbol{\gamma}_\times^{a+}\boldsymbol{E}_0=\boldsymbol{\gamma}_\times^{a-}\boldsymbol{E}_a=\mathrm{i}\omega\mu_0L\boldsymbol{M}^a,$$

in order to automatically satisfy the transmission conditions of problem (2) and recalling the definition (4) of $\boldsymbol{E}^{\rm inc}$, the above Stratton-Chu formulas become

$$\begin{aligned} (\mathrm{i}\mu_0\omega)^{-1}\boldsymbol{E}_0&=\boldsymbol{\Phi}[\boldsymbol{J}_{\rm s}]-\sum_{a=1}^M\big(\boldsymbol{\mathcal{S}}_0^a[\boldsymbol{J}^a]+\boldsymbol{\mathcal{D}}_0^a[\boldsymbol{M}^a]\big) && \text{in } \Omega_0,\\ (\mathrm{i}\mu_0\omega)^{-1}\boldsymbol{E}_a&=\mu_{{\rm r}a}\boldsymbol{\mathcal{S}}_a^a[\boldsymbol{J}^a]+\boldsymbol{\mathcal{D}}_a^a[\boldsymbol{M}^a] && \text{in } \Omega_a. \end{aligned} \tag{10}$$

The magnetic field $\boldsymbol{H}=(\mathrm{i}\mu_0\omega)^{-1}\mathbf{rot}\,\boldsymbol{E}$ is then given, applying (9) to (10), by

$$\begin{aligned} \boldsymbol{H}_0&=\mathbf{rot}\,\boldsymbol{\Phi}[\boldsymbol{J}_{\rm s}]-\frac{1}{L}\sum_{a=1}^M\big(\boldsymbol{\mathcal{D}}_0^a[\boldsymbol{J}^a]+(\kappa_0L)^2\boldsymbol{\mathcal{S}}_0^a[\boldsymbol{M}^a]\big) && \text{in } \Omega_0,\\ \boldsymbol{H}_a&=\frac{1}{L}\Big(\boldsymbol{\mathcal{D}}_a^a[\boldsymbol{J}^a]+\mu_{{\rm r}a}^{-1}(\kappa_aL)^2\boldsymbol{\mathcal{S}}_a^a[\boldsymbol{M}^a]\Big) && \text{in } \Omega_a. \end{aligned} \tag{11}$$

1.3 PMCHWT integral formulation. We additionally know (see [8]) that the trace operators $\boldsymbol{\gamma}_\times^{a-}$, $\boldsymbol{\gamma}_N^{a-}$ (respectively $\boldsymbol{\gamma}_\times^{a+}$, $\boldsymbol{\gamma}_N^{a+}$) introduced in (3) have extensions as linear continuous operators from $\boldsymbol{H}(\mathbf{rot}\,\mathbf{rot}\,,\Omega_a)$ (respectively $\boldsymbol{H}_{\mathrm{loc}}(\mathbf{rot}\,\mathbf{rot}\,,\mathbb{R}^3\backslash\overline{\Omega_a})$) to $\boldsymbol{\mathcal{V}}^a$. The boundary traces of $\boldsymbol{\mathcal{S}}_\ell^b, \boldsymbol{\mathcal{D}}_\ell^b$ under $\boldsymbol{\gamma}_\times^{\pm a}$ and $\boldsymbol{\gamma}_N^{\pm a}$ are therefore well-defined for any $1\le a,b\le M$, allowing to introduce the $\boldsymbol{\mathcal{V}}^a\to\boldsymbol{\mathcal{V}}^a$ boundary integral operators

$$\mathsf{S}_\ell^{ab} := \tfrac{1}{2}(\boldsymbol{\gamma}_\times^{a+}+\boldsymbol{\gamma}_\times^{a-})\boldsymbol{\mathcal{S}}_\ell^b, \qquad \mathsf{D}_\ell^{ab} := \tfrac{1}{2}(\boldsymbol{\gamma}_\times^{a+}+\boldsymbol{\gamma}_\times^{a-})\boldsymbol{\mathcal{D}}_\ell^b. \tag{12}$$

Then, using well-known jump properties [9], $\boldsymbol{\mathcal{S}}_\ell^a, \boldsymbol{\mathcal{D}}_\ell^a$ have their boundary traces under $\boldsymbol{\gamma}_\times^{a\pm}$ given by

$$\boldsymbol{\gamma}_\times^{a+}\boldsymbol{\mathcal{S}}_\ell^a = \mathsf{S}_\ell^{aa}, \qquad \boldsymbol{\gamma}_\times^{a-}\boldsymbol{\mathcal{S}}_\ell^a = \mathsf{S}_\ell^{aa}, \qquad \boldsymbol{\gamma}_\times^{a+}\boldsymbol{\mathcal{D}}_\ell^a = \mathsf{D}_\ell^{aa} - \tfrac{1}{2}\mathsf{I}, \qquad \boldsymbol{\gamma}_\times^{a-}\boldsymbol{\mathcal{D}}_\ell^a = \mathsf{D}_\ell^{aa} + \tfrac{1}{2}\mathsf{I},$$

while their boundary traces under $\boldsymbol{\gamma}_\times^{b\pm}$ are straightforward (since $\boldsymbol{\mathcal{S}}_\ell^a, \boldsymbol{\mathcal{D}}_\ell^a$ are $C^\infty(\mathbb{R}^3\setminus\Gamma_a;\mathbb{C}^3)$ functions and $\Gamma_a\cap\Gamma_b=\emptyset$ in this case). Moreover, the interrelations (9) imply $L\boldsymbol{\gamma}_N\boldsymbol{\mathcal{S}}_\ell^a = \boldsymbol{\gamma}_\times\boldsymbol{\mathcal{D}}_\ell^a$ and $L\boldsymbol{\gamma}_N\boldsymbol{\mathcal{D}}_\ell^a = (\kappa_\ell L)^2\boldsymbol{\gamma}_\times\boldsymbol{\mathcal{S}}_\ell^a$, so that the boundary traces of $\boldsymbol{\mathcal{S}}_\ell^a, \boldsymbol{\mathcal{D}}_\ell^a$ under $\boldsymbol{\gamma}_N^{a\pm}$ are given by

$$L\boldsymbol{\gamma}_N^{a+}\boldsymbol{\mathcal{S}}_\ell^a = \mathsf{D}_\ell^{aa} - \tfrac{1}{2}\mathsf{I}, \qquad L\boldsymbol{\gamma}_N^{a-}\boldsymbol{\mathcal{S}}_\ell^a = \mathsf{D}_\ell^{aa} + \tfrac{1}{2}\mathsf{I}, \qquad L\boldsymbol{\gamma}_N^{a+}\boldsymbol{\mathcal{D}}_\ell^a = \kappa_\ell^2\mathsf{S}_\ell^{aa}, \qquad L\boldsymbol{\gamma}_N^{a-}\boldsymbol{\mathcal{D}}_\ell^a = \kappa_\ell^2\mathsf{S}_\ell^{aa}.$$

On evaluating the discontinuities $\boldsymbol{\gamma}_\times^{a+}\boldsymbol{E}_0 - \boldsymbol{\gamma}_\times^{a-}\boldsymbol{E}_a$ and $\boldsymbol{\gamma}_N^{a+}\boldsymbol{E}_0 - \boldsymbol{\gamma}_N^{a-}\boldsymbol{E}_a$ $(1\le a\le M)$ of the boundary traces of the Stratton-Chu formulas (10), using the foregoing definitions and properties and introducing the source terms defined by

$$\boldsymbol{f}_{\mathrm{s}}^a := \boldsymbol{\gamma}_\times^{a+}\boldsymbol{\Phi}[\boldsymbol{J}_{\mathrm{s}}], \qquad \boldsymbol{g}_{\mathrm{s}}^a := L\boldsymbol{\gamma}_N^{a+}\boldsymbol{\Phi}[\boldsymbol{J}_{\mathrm{s}}], \tag{13}$$

we arrive at the governing system of integral equations

$$\begin{aligned}
\mu_{\mathrm{r}a}\mathsf{S}_a^{aa}[\boldsymbol{J}^a] + \mathsf{D}_a^{aa}[\boldsymbol{M}^a] + \sum_{b=1}^M \big(\mathsf{S}_0^{ab}[\boldsymbol{J}^b] + \mathsf{D}_0^{ab}[\boldsymbol{M}^b]\big) &= \boldsymbol{f}_{\mathrm{s}}^a,\\
\mathsf{D}_a^{aa}[\boldsymbol{J}^a] + \mu_{\mathrm{r}a}^{-1}(\kappa_a L)^2\mathsf{S}_a^{aa}[\boldsymbol{M}^a] + \sum_{b=1}^M \big(\mathsf{D}_0^{ab}[\boldsymbol{J}^b] + (\kappa_0 L)^2\mathsf{S}_0^{ab}[\boldsymbol{M}^b]\big) &= \boldsymbol{g}_{\mathrm{s}}^a
\end{aligned} \tag{14}$$

for $(\boldsymbol{J}^1,\boldsymbol{M}^1,\dots,\boldsymbol{J}^M,\boldsymbol{M}^M)$, known as the Poggio-Miller-Chang-Harrington-Wu-Tsai (PMCHWT) integral formulation [25] for the scattering problem (2). As expected, all operators linking two distinct bodies Ω_a,Ω_b $(a\neq b)$ in problem (14) involve solely the vacuum medium.

1.4 Helmholtz–Hodge decomposition, weak formulation. We now introduce a Helmholtz–Hodge decomposition $\boldsymbol{\mathcal{V}}^a = \boldsymbol{\mathcal{V}}_{\mathrm{L}}^a \oplus \boldsymbol{\mathcal{V}}_{\mathrm{T}}^a$ of each space $\boldsymbol{\mathcal{V}}^a$, where $\boldsymbol{\mathcal{V}}_{\mathrm{L}}^a := \big\{\boldsymbol{u}\in\boldsymbol{\mathcal{V}}^a : \mathrm{div}_S\boldsymbol{u}=0\big\}$ (see [8]), and the corresponding additive decompositions $\boldsymbol{J}^a = \boldsymbol{J}_{\mathrm{L}}^a + \boldsymbol{J}_{\mathrm{T}}^a$ and $\boldsymbol{M}^a = \boldsymbol{M}_{\mathrm{L}}^a + \boldsymbol{M}_{\mathrm{T}}^a$ of the unknown surface currents, with $\boldsymbol{J}_{\mathrm{L}}^a, \boldsymbol{M}_{\mathrm{L}}^a \in \boldsymbol{\mathcal{V}}_{\mathrm{L}}^a$ and $\boldsymbol{J}_{\mathrm{T}}^a, \boldsymbol{M}_{\mathrm{T}}^a \in \boldsymbol{\mathcal{V}}_{\mathrm{T}}^a$. Discrete Helmholtz–Hodge decompositions of finite-dimensional BE approximation spaces exist in several forms, such as the well-known *loop–tree* decomposition (to which the L,T subscripts introduced above refer) used in Sec. 4, and are often used for circumventing low-frequency breakdown in integral equation methods for electromagnetic scattering (see e.g. [10]). Recall that all bodies are for now assumed to be simply-connected, in which case we have $\boldsymbol{\mathcal{V}}_{\mathrm{L}}^a = \mathbf{rot}_S\big(H^{1/2}(\Gamma_a)\big)$ for each interface, where $\mathbf{rot}_S$ is the surface curl operator [7].

In its continuous form, this decomposition will play an essential role in the asymptotic expansions to follow. In particular, the single-layer Maxwell integral operators S_ℓ^{ab} are decomposed as

$$\begin{aligned}
&\mathsf{S}_\ell^{ab} = \mathsf{A}_\ell^{ab} + (\kappa_a L)^{-2}\mathsf{K}_\ell^{ab}\\
&\qquad\text{with}\qquad \mathsf{A}_\ell^{ab} := \tfrac{1}{2}(\boldsymbol{\gamma}_\times^{a+}+\boldsymbol{\gamma}_\times^{a-})\boldsymbol{\mathcal{A}}_\ell^b, \qquad \mathsf{K}_\ell^{ab} := \tfrac{1}{2}(\boldsymbol{\gamma}_\times^{a+}+\boldsymbol{\gamma}_\times^{a-})\boldsymbol{\mathcal{K}}_\ell^b \qquad (\ell=0,1,\dots,M),
\end{aligned} \tag{15}$$

allowing to take advantage of the fact that $\big\langle\boldsymbol{\phi}^a, \mathsf{K}_\ell^{ab}\boldsymbol{\phi}^b\big\rangle_\times^a = 0$ if either $\boldsymbol{\phi}^a\in\boldsymbol{\mathcal{V}}_{\mathrm{L}}^a$ or $\boldsymbol{\phi}^b\in\boldsymbol{\mathcal{V}}_{\mathrm{L}}^b$, where the twisted inner product $\big\langle\cdot,\cdot\big\rangle_\times^a$ on each Γ_a is defined by

$$\big\langle\boldsymbol{u},\boldsymbol{v}\big\rangle_\times^a := -\int_{\Gamma_a}\boldsymbol{u}\cdot(\boldsymbol{v}\times\boldsymbol{n})\,\mathrm{d}S \qquad 1\le a\le M.$$

Using the Helmholtz-Hodge decomposition and emphasizing the contribution of each medium in the integral operators, the weak formulation of the PMCHWT system (14) is: find $\big(\boldsymbol{X}^1,\dots,\boldsymbol{X}^M\big)\in\mathbb{V}$ such that

$$\sum_{a=1}^M\sum_{b=1}^M\big\langle\widetilde{\boldsymbol{X}}^a, (\boldsymbol{\mathcal{Z}}_a^{aa}\delta_{ab}+\boldsymbol{\mathcal{Z}}_0^{ab})\boldsymbol{X}^b\big\rangle_\times^a = \sum_{a=1}^M\big\langle\widetilde{\boldsymbol{X}}^a,\boldsymbol{Y}^a\big\rangle_\times^a \qquad \text{for all } \big(\widetilde{\boldsymbol{X}}^1,\dots,\widetilde{\boldsymbol{X}}^M\big)\in\mathbb{V}, \tag{16}$$

where $\mathbb{V}$ is the Cartesian product function space $\mathbb{V} := \big(\boldsymbol{\mathcal{V}}_{\mathrm{L}}^1 \times \boldsymbol{\mathcal{V}}_{\mathrm{T}}^1 \times \boldsymbol{\mathcal{V}}_{\mathrm{L}}^1 \times \boldsymbol{\mathcal{V}}_{\mathrm{T}}^1\big) \times \ldots \times \big(\boldsymbol{\mathcal{V}}_{\mathrm{L}}^M \times \boldsymbol{\mathcal{V}}_{\mathrm{T}}^M \times \boldsymbol{\mathcal{V}}_{\mathrm{L}}^M \times \boldsymbol{\mathcal{V}}_{\mathrm{T}}^M\big)$, each operator matrix $\boldsymbol{\mathcal{Z}}_\ell^{ab}$ is given in block form by

$$\boldsymbol{\mathcal{Z}}_\ell^{ab} = \begin{bmatrix} \mu_{\mathrm{r}\ell}\mathbf{A}_\ell^{ab} & \mu_{\mathrm{r}\ell}\mathbf{A}_\ell^{ab} & \mathbf{D}_{\ell\star}^{ab} & \mathbf{D}_\ell^{ab} \\ \mu_{\mathrm{r}\ell}\mathbf{A}_\ell^{ab} & \mu_{\mathrm{r}\ell}\mathbf{S}_\ell^{ab} & \mathbf{D}_\ell^{ab} & \mathbf{D}_\ell^{ab} \\ \mathbf{D}_{\ell\star}^{ab} & \mathbf{D}_\ell^{ab} & \mu_{\mathrm{r}\ell}^{-1}(\kappa_\ell L)^2\mathbf{A}_\ell^{ab} & \mu_{\mathrm{r}\ell}^{-1}(\kappa_\ell L)^2\mathbf{A}_\ell^{ab} \\ \mathbf{D}_\ell^{ab} & \mathbf{D}_\ell^{ab} & \mu_{\mathrm{r}\ell}^{-1}(\kappa_\ell L)^2\mathbf{A}_\ell^{ab} & \mu_{\mathrm{r}\ell}^{-1}(\kappa_\ell L)^2\mathbf{S}_\ell^{ab} \end{bmatrix}, \tag{17}$$

the unknowns $\boldsymbol{X}^a$, test function $\widetilde{\boldsymbol{X}}^a$ and right-hand sides $\boldsymbol{Y}^a$ are given, in corresponding block form, by

$$\boldsymbol{X}^a = \big\{\boldsymbol{J}_{\mathrm{L}}^a, \boldsymbol{J}_{\mathrm{T}}^a, \boldsymbol{M}_{\mathrm{L}}^a, \boldsymbol{M}_{\mathrm{T}}^a\big\}^{\mathrm{T}}, \qquad \widetilde{\boldsymbol{X}}^a = \big\{\widetilde{\boldsymbol{J}}_{\mathrm{L}}^a, \widetilde{\boldsymbol{J}}_{\mathrm{T}}^a, \widetilde{\boldsymbol{M}}_{\mathrm{L}}^a, \widetilde{\boldsymbol{M}}_{\mathrm{T}}^a\big\}^{\mathrm{T}}, \qquad \boldsymbol{Y}^a = \big\{\boldsymbol{f}_{\mathrm{s}}^a, \boldsymbol{f}_{\mathrm{s}}^a, \boldsymbol{g}_{\mathrm{s}}^a, \boldsymbol{g}_{\mathrm{s}}^a\big\}^{\mathrm{T}}. \tag{18}$$

For any a, b, ℓ, the operator matrices (17) verify $\big\langle \widetilde{\boldsymbol{X}}^a, \boldsymbol{\mathcal{Z}}_\ell^{ab}\boldsymbol{X}^b\big\rangle_\times^a = \big\langle \boldsymbol{X}^b, \boldsymbol{\mathcal{Z}}_\ell^{ba}\widetilde{\boldsymbol{X}}^a\big\rangle_\times^a$, so that the global operator matrix for the weak formulation (16) is complex symmetric (not Hermitian).

In adddition, the operator $\mathbf{D}_{\ell\star}^{ab}$ in (17) is a modified version of $\mathbf{D}_\ell^{ab}$ with $G(\cdot;\kappa_\ell)$ replaced by $G_\star(\cdot;\kappa_\ell) := G(\cdot;\kappa_\ell) - G(\cdot;0)$, which is easily verified to be nonsingular at the origin. The subtracted term thus introduced vanishes in theory (as shown later, see Lemma 2d), but may in practice pollute the discrete solution process, making this modification both valid and computationally beneficial.

1.5 Solution post-processing.

Eddy current nondestructive testing exploits measurements of the normalized impedance variation [2]

$$\Delta Z := \mathrm{i}\omega\mu_0 \sum_a \int_{\Gamma_a} \big(\boldsymbol{J}^a \cdot \boldsymbol{\Phi}[\hat{\boldsymbol{J}}_{\mathrm{s}}] + \boldsymbol{M}^a \cdot L\mathbf{rot}\,\boldsymbol{\Phi}[\hat{\boldsymbol{J}}_{\mathrm{s}}]\big)\,\mathrm{d}S_a = \mathrm{i}\omega\mu_0 \sum_a \Big(\big\langle \boldsymbol{J}^a, \boldsymbol{f}_{\mathrm{s}}^a\big\rangle_\times^a + \big\langle \boldsymbol{M}^a, \boldsymbol{g}_{\mathrm{s}}^a\big\rangle_\times^a\Big) \tag{19}$$

(with $\hat{\boldsymbol{J}}_{\mathrm{s}}$ given by (7) and $\boldsymbol{f}_{\mathrm{s}}^a, \boldsymbol{g}_{\mathrm{s}}^a$ defined in terms of $\hat{\boldsymbol{J}}_{\mathrm{s}}$) which reflects the relative electromagnetic field perturbation induced by the conducting bodies Ω_a. The values of $\boldsymbol{E}$ and $\boldsymbol{H}$ at locations in the vacuum Ω_0 may also be of interest. Hereafter we will provide asymptotic approximations for those quantities in addition to the surface current densities solving the PMCHWT problem (14).

2 Expansion of the PMCHWT problem.

We define the dimensionless parameter

$$\eta := \kappa_0 L, \tag{20}$$

where L is the characteristic length already used in (8). Our primary goal is to approximate the Maxwell (integral equation) model (16) for low frequencies (i.e. when $\eta \ll 1$) by seeking an expansion in powers of η of the surface currents $\boldsymbol{J}^a, \boldsymbol{M}^a$ $(1 \le a \le M)$ in situations where each of the M bounded objects Ω_a is either non-conducting (NC), mildly conducting (MC) or highly conducting (HC). Each object type is here defined in terms of the conductivity σ_a being assumed to have the respective form

$$\sigma_a = 0 \quad (a \in \mathcal{N}), \qquad \sigma_a = \xi_a^2\sigma_{\mathrm{ref}} \quad (a \in \mathcal{M}), \qquad \sigma_a = \eta^{-1}\xi_a^2\sigma_{\mathrm{ref}} \quad (a \in \mathcal{C}) \tag{21}$$

where we have introduced the lists $\mathcal{N}, \mathcal{M}, \mathcal{C}$ of indices of bodies of type NC, MC, HC, respectively (e.g. $\{\Omega_a,\ a \in \mathcal{N}\}$ gathers all NC bodies) with $\mathcal{N} \cup \mathcal{M} \cup \mathcal{C} = \{1, \ldots, M\}$, and each dimensionless factor ξ_a is fixed (i.e. independent on η). The characteristic conductivity σ_{ref} in (21) is given by

$$\sigma_{\mathrm{ref}} := \tfrac{1}{L}\sqrt{\varepsilon_0/\mu_0}.$$

The definition (20) of η characterizes low frequencies and allows for a unified asymptotic framework where HC, MC and NC objects may coexist, whereas $\gamma := \sqrt{\omega\varepsilon_0/\sigma}$ used in [6] directly combined low-frequency and large-conductivity asymptotics. Moreover, the conductivity scalings (21) are such that for a HC object with conductivity σ_a we have $\gamma = \eta/\xi_a$, and we then find that $\xi_a = \sqrt{2/\mu_{\mathrm{r}a}}L/\delta_a$ (where $\delta_a = \sqrt{2/\omega\sigma_a\mu_0\mu_{\mathrm{r}a}}$ is the skin depth for the HC material of Ω_a), i.e. coincides with the parameter ξ introduced in [6]. The EC regime (in [6] as well as here) is characterized by a fixed value of ξ_a, reflecting the fact that ECT experiments are calibrated with respect to a chosen skin depth. This makes the forthcoming small-η asymptotic equivalent to the small-γ asymptotics of [6] when only HC bodies are present. We observe in passing that the wavenumber approximation used in [11] corresponds to the present MC case.

2.1 Expansion of wavenumbers, fundamental solutions and operators. The integral operator matrix given by (17) and the right-hand side given by (18) depend on η through the wavenumbers κ_a, for which (in addition to (20) for the vacuum) we have

$$\begin{aligned}
&\kappa_a L = \sqrt{\mu_{\mathrm{r}a}(\mathrm{i}\xi_a^2+\varepsilon_{\mathrm{r}a}^{\mathrm{d}}\eta^2)} = q_a + O(\eta^2), && q_a := \xi_a\sqrt{\mathrm{i}\mu_{\mathrm{r}a}} && (a\in\mathcal{C}),\\
&\kappa_a L = q_a\eta, && q_a := \sqrt{\varepsilon_{\mathrm{r}a}^{\mathrm{d}}\mu_{\mathrm{r}a}} && (a\in\mathcal{N}),\\
&\kappa_a L = \sqrt{\mu_{\mathrm{r}a}(\mathrm{i}\xi_a^2\eta+\varepsilon_{\mathrm{r}a}^{\mathrm{d}}\eta^2)} = \eta^{1/2}q_a+\eta^{3/2}q_a^3q_a'+O(\eta^2), && q_a := \xi_a\sqrt{\mathrm{i}\mu_{\mathrm{r}a}},\ q_a' := \frac{\varepsilon_{\mathrm{r}a}^{\mathrm{d}}\mu_{\mathrm{r}a}}{2q_a^4} && (a\in\mathcal{M}).
\end{aligned} \tag{22}$$

HC materials. For this case, κ_a does not vanish as $\eta\to 0$. The Helmholtz fundamental solution and its gradient admit for this case the expansions

$$G(\boldsymbol{z};\kappa_a) = G_{0,a}^{\mathrm{C}}(\boldsymbol{z}) + O(\eta^2), \qquad L\boldsymbol{\nabla}G(\boldsymbol{z};\kappa_a) = H_{0,a}^{\mathrm{C}}(\boldsymbol{z}) + O(\eta^2) \qquad (a\in\mathcal{C}) \tag{23}$$

with

$$G_{0,a}^{\mathrm{C}}(\boldsymbol{z}) = \frac{e^{\mathrm{i}q_a|\boldsymbol{z}|/L}}{4\pi|\boldsymbol{z}|}, \qquad H_{0,a}^{\mathrm{C}}(\boldsymbol{z}) = \frac{e^{\mathrm{i}q_a|\boldsymbol{z}|/L}}{4\pi|\boldsymbol{z}|^3}\big(\mathrm{i}q_a|\boldsymbol{z}|-L\big)\boldsymbol{z}$$

Other materials. For the vacuum and the NC or MC materials, κ_a vanishes as $\eta\to 0$ and expansions of the Helmholtz fundamental solution and its gradient in powers of η are conveniently found from the generic expansions

$$\begin{aligned}
G(\boldsymbol{z};\kappa) &= G_0(\boldsymbol{z}) + \kappa L G_1 + (\kappa L)^2 G_2(\boldsymbol{z}) + (\kappa L)^3 G_3(\boldsymbol{z}) + O(\kappa^4)\\
L\boldsymbol{\nabla}G(\boldsymbol{z};\kappa) &= \big[H_0(\boldsymbol{z}) + (\kappa L)^2 H_2(\boldsymbol{z}) + (\kappa L)^3 H_3 + (\kappa L)^4 H_4(\boldsymbol{z}) + (\kappa L)^5 H_5(\boldsymbol{z})\big]\boldsymbol{z} + O(\kappa^5)
\end{aligned} \tag{24}$$

whose coefficients

$$\begin{aligned}
&G_0(\boldsymbol{z}) = \frac{1}{4\pi|\boldsymbol{z}|}, && G_1 = \frac{\mathrm{i}}{4\pi L}, && G_2(\boldsymbol{z}) = \frac{-|\boldsymbol{z}|}{8\pi L^2}, && G_3(\boldsymbol{z}) = \frac{-\mathrm{i}|\boldsymbol{z}|^2}{24\pi L^3},\\
&H_0(\boldsymbol{z}) = \frac{-L}{4\pi|\boldsymbol{z}|^3}, && H_2(\boldsymbol{z}) = \frac{-1}{8\pi L|\boldsymbol{z}|}, && H_3 = \frac{-\mathrm{i}}{12\pi L^2}, && H_4(\boldsymbol{z}) = \frac{|\boldsymbol{z}|}{32\pi L^3}, && H_5(\boldsymbol{z}) = \frac{|\boldsymbol{z}|^2}{120\pi L^4}
\end{aligned}$$

do not depend on material parameters. We note that $G_0 = G(\cdot;0)$ is the Laplace fundamental solution and G_1, H_3 are constant w.r.t. $\boldsymbol{z}$. Setting $\kappa=\kappa_a$ and using $\kappa_0 L = \eta$ for $a=0$ or expansions (22) for $a\in\mathcal{N}$ or $a\in\mathcal{M}$, we obtain

$$\begin{aligned}
G(\boldsymbol{z};\kappa_a) &= G_0(\boldsymbol{z}) + \eta q_a G_1 + \eta^2 q_a^2 G_2(\boldsymbol{z}) + \eta^3 q_a^3 G_3(\boldsymbol{z}) + O(\eta^4) && (a=0,\ a\in\mathcal{N}),\\
G(\boldsymbol{z};\kappa_a) &= G_0(\boldsymbol{z}) + \eta^{1/2} q_a G_1 + \eta q_a^2 G_2(\boldsymbol{z}) + \eta^{3/2} q_a^3\big[G_3(\boldsymbol{z}) + q_a' G_1\big] + O(\eta^2) && (a\in\mathcal{M})\\
L\boldsymbol{\nabla}G(\boldsymbol{z};\kappa_a) &= \big[H_0(\boldsymbol{z}) + \eta^2 q_a^2 H_2(\boldsymbol{z}) + \eta^3 q_a^3 H_3\big]\,\boldsymbol{z} + O(\eta^4) && (a=0,\ a\in\mathcal{N}),\\
L\boldsymbol{\nabla}G(\boldsymbol{z};\kappa_a) &= \big[H_0(\boldsymbol{z}) + \eta q_a^2 H_2(\boldsymbol{z}) + \eta^{3/2} q_a^3 H_3 + \eta^2 q_a^4\big(H_4(\boldsymbol{z}) + 2q_a' H_2(\boldsymbol{z})\big)\\
&\qquad + \eta^{5/2} q_a^5\big(H_5(\boldsymbol{z}) + 3q_a' H_3\big)\big]\,\boldsymbol{z} + O(\eta^3) && (a\in\mathcal{M}).
\end{aligned} \tag{25}$$

where q_a is given by $q_a = 1$ for the surrounding air ($a=0$) and by (22) in the other cases.

In turn, expansions of the source terms $\boldsymbol{f}_{\mathrm{s}}^a, \boldsymbol{g}_{\mathrm{s}}^a$ and the integral operators $\mathbf{A}_\ell^{ab}$, $\mathbf{D}_\ell^{ab}$ and $\mathbf{K}_\ell^{ab}$ introduced in (12) and (15) can be derived from expansions (23) for HC media ($\ell\in\mathcal{C}$), and from expansions (24) for all other media noting, for $\mathbf{D}_\ell^{ab}$, that $\mathbf{rot}_{\boldsymbol{x}}\big(G(\boldsymbol{x}-\boldsymbol{x}';\kappa_a)\boldsymbol{u}(\boldsymbol{x}')\big) = \boldsymbol{\nabla}G(\boldsymbol{x}-\boldsymbol{x}';\kappa_a)\times\boldsymbol{u}(\boldsymbol{x}'))$. In particular, all operator expansions in the latter case involve operator-valued coefficients based on the set of kernels G_p and H_p appearing in (24), which are naturally associated with the vacuum medium.

2.2 Some useful properties of potentials and integral operators. On the basis of the foregoing expansions of κ_a and $G(\cdot;\kappa_a)$, the following properties of the incident field and of integral operators for media of type other than HC, which will prove useful in deriving the expansion of problem (14), are obtained:

Lemma 1. *Let $\boldsymbol{J}_s$ be such that $\mathrm{div}\,\boldsymbol{J}_s = 0$ in D and $\boldsymbol{J}_s\cdot\boldsymbol{n} = 0$ on ∂D. Let $\boldsymbol{\Phi}_{(m)}$ be the volume potential obtained by replacing $G(\cdot;\kappa_0)$ with G_m, as given in (24), in (5), and $\boldsymbol{g}^a_{s(m)}$ the corresponding source term resulting from (13). Then:*

(a) $\boldsymbol{\Phi}_{(1)}[\boldsymbol{J}_s] = \boldsymbol{0}$.

(b) $\big\langle \boldsymbol{\phi}^a_L,\, \boldsymbol{g}^a_{s(0)} \big\rangle^a_\times = 0$ *for any* $\boldsymbol{\phi}^a_L \in \boldsymbol{\mathcal{V}}^a_{\mathrm{L}}$ *if* Γ_a *is simply-connected.*

(c) $\big\langle \boldsymbol{\phi}^a_L,\, \boldsymbol{g}^a_{s(3)} \big\rangle^a_\times = 0$ *for any* $\boldsymbol{\phi}^a_L \in \boldsymbol{\mathcal{V}}^a_{\mathrm{L}}$ *if* Γ_a *is simply-connected.*

Lemma 2. *For any $1 \le a, b \le M$, let $\mathsf{A}^{ab}_{(m)}$ and $\mathsf{D}^{ab}_{(m)}$ be the integral operators respectively defined by (15) and (12) with G replaced by G_m as given in (24). Then:*

(a) $\mathsf{A}^{ab}_{(1)}\boldsymbol{\phi}^b_L = \boldsymbol{0}$ *for any* $\boldsymbol{\phi}^b_L \in \boldsymbol{\mathcal{V}}^b_{\mathrm{L}}$.

(b) $\mathsf{D}^{ab}_{(1)}\boldsymbol{\phi}^b = \boldsymbol{0}$ *and* $\mathsf{K}^{ab}_{(1)}\boldsymbol{\phi}^b = \boldsymbol{0}$ *for any* $\boldsymbol{\phi}^b \in \boldsymbol{\mathcal{V}}^b$.

(c) $\big\langle \boldsymbol{\phi}^a_L,\, \mathsf{A}^{ab}_{(1)}\boldsymbol{\phi}^b \big\rangle^a_\times = 0$ *for any* $\boldsymbol{\phi}^a_L \in \boldsymbol{\mathcal{V}}^a_{\mathrm{L}}$ *and* $\boldsymbol{\phi}^b \in \boldsymbol{\mathcal{V}}^b$.

(d) $\big\langle \boldsymbol{\phi}^a_L,\, \mathsf{D}^{ab}_{(0)}\boldsymbol{\phi}^b_L \big\rangle^a_\times = 0$ *for any* $\boldsymbol{\phi}^a_L \in \boldsymbol{\mathcal{V}}^a_{\mathrm{L}}$ *and* $\boldsymbol{\phi}^b_L \in \boldsymbol{\mathcal{V}}^b_{\mathrm{L}}$ *if either* Γ_a *or* Γ_b *is simply-connected.*

(e) $\big\langle \boldsymbol{\phi}^a_L,\, \mathsf{D}^{ab}_{(3)}\boldsymbol{\phi}^b_L \big\rangle^a_\times = 0$ *for any* $\boldsymbol{\phi}^a_L \in \boldsymbol{\mathcal{V}}^a_{\mathrm{L}}$ *and* $\boldsymbol{\phi}^b_L \in \boldsymbol{\mathcal{V}}^b_{\mathrm{L}}$ *if either* Γ_a *or* Γ_b *is simply-connected.*

Proof of Lemmas 1 and 2. See Section A.1. □

In particular, the operator $\mathsf{D}^{ab}_{\ell\star}$ appearing in the definition (17) of $\boldsymbol{\mathcal{Z}}^{ab}_\ell$ is given by

$$\mathsf{D}^{ab}_{\ell\star} := \mathsf{D}^{ab}_{\ell} - \mathsf{D}^{ab}_{(0)} \tag{26}$$

and Lemma 2d justifies that $\mathsf{D}^{ab}_{(0)}$ vanishes under the weak form at the corresponding locations in $\boldsymbol{\mathcal{Z}}^{ab}_\ell$.

2.3 Rescaled PMCHWT problem.

As previously observed in [6] on the corresponding formulation for a HC body surrounded by vacuum, the integral operators involved in the weak form (16) of the PMCHWT problem have varying (and in some cases negative) leading orders in η. Here, using expansions (23) for HC media and expansions (24) for the other media types, the operator matrices $\boldsymbol{\mathcal{Z}}^{ab}_\ell$ defined by (17) and the right-hand sides $\boldsymbol{Y}^a$ defined by (18) are found to have leading orders given by

$$\boldsymbol{\mathcal{Z}}^{ab}_\ell = O\left(\begin{bmatrix} 1 & 1 & 1 & 1 \\ 1 & 1 & 1 & 1 \\ 1 & 1 & 1 & 1 \\ 1 & 1 & 1 & 1 \end{bmatrix}\right), \qquad O\left(\begin{bmatrix} 1 & 1 & \eta^2 & 1 \\ 1 & \eta^{-2} & 1 & 1 \\ \eta^2 & 1 & \eta^2 & \eta^2 \\ 1 & 1 & \eta^2 & 1 \end{bmatrix}\right), \qquad O\left(\begin{bmatrix} 1 & 1 & \eta & 1 \\ 1 & \eta^{-1} & 1 & 1 \\ \eta & 1 & \eta & \eta \\ 1 & 1 & \eta & 1 \end{bmatrix}\right), \tag{27a}$$

(HC) (vacuum or NC) (MC)

$$\boldsymbol{Y}^a = O\big(\{1 \;\; 1 \;\; \eta^2 \;\; 1\}^{\mathrm{T}}\big). \tag{27b}$$

Prior to a complete derivation of its sought expansion, problem (16) is rescaled on the basis of (27a,b) so that its global operator matrix becomes well-behaved as $\eta \to 0$. This is accomplished by (i) using rescaled test functions $\boldsymbol{\Pi}^a_\eta \widetilde{\boldsymbol{X}}^a$ and (ii) introducing rescaled unknowns via $\boldsymbol{X}^b = \boldsymbol{\Sigma}_\eta \widehat{\boldsymbol{X}}^b_\eta$ into problem (16), with the scaling block-diagonal operators defined by

$$\begin{aligned} &\boldsymbol{\Pi}^a_\eta \widetilde{\boldsymbol{X}}^a = \big\{ \widetilde{\boldsymbol{J}}^a_{\mathrm{L}},\, \widetilde{\boldsymbol{J}}^a_{\mathrm{T}},\, \eta^{-p}\widetilde{\boldsymbol{M}}^a_{\mathrm{L}},\, \widetilde{\boldsymbol{M}}^a_{\mathrm{T}} \big\}^{\mathrm{T}} \qquad \text{with} \;\; p=0 \;\; (a\in\mathcal{C}), \;\; p=1 \;\; (a\in\mathcal{M}), \;\; p=2 \;\; (a\in\mathcal{N}), \\ &\boldsymbol{\Sigma}_\eta \widehat{\boldsymbol{X}}^a_\eta = \big\{ \widehat{\boldsymbol{J}}^a_{\mathrm{L}},\, \eta^2\widehat{\boldsymbol{J}}^a_{\mathrm{T}},\, \widehat{\boldsymbol{M}}^a_{\mathrm{L}},\, \widehat{\boldsymbol{M}}^a_{\mathrm{T}} \big\}^{\mathrm{T}}. \end{aligned} \tag{28}$$

As a result, problem (16) is recast as: find $\big(\widehat{\boldsymbol{X}}^1_\eta, \ldots, \widehat{\boldsymbol{X}}^M_\eta\big) \in \mathbb{V}$ such that

$$\sum_{a=1}^{M}\sum_{b=1}^{M} \big\langle \widetilde{\boldsymbol{X}}^a,\, (\widehat{\boldsymbol{\mathcal{Z}}}^{aa}_{\eta,a}\delta_{ab} + \widehat{\boldsymbol{\mathcal{Z}}}^{ab}_{\eta,0})\widehat{\boldsymbol{X}}^a_\eta \big\rangle^a_\times = \sum_{a=1}^{M} \big\langle \widetilde{\boldsymbol{X}}^a,\, \widehat{\boldsymbol{Y}}^a_\eta \big\rangle^a_\times \qquad \text{for all } \big(\widetilde{\boldsymbol{X}}^1, \ldots, \widetilde{\boldsymbol{X}}^M\big) \in \mathbb{V}, \tag{29}$$

where $\widehat{\boldsymbol{X}}^a_\eta := \{\widehat{\boldsymbol{J}}^a_{\mathrm{L}}, \widehat{\boldsymbol{J}}^a_{\mathrm{T}}, \widehat{\boldsymbol{M}}^a_{\mathrm{L}}, \widehat{\boldsymbol{M}}^a_{\mathrm{T}}\}^{\mathrm{T}}$ for each body and the rescaled operator matrices and right-hand side are given by

$$\widehat{\boldsymbol{\mathcal{Z}}}^{ab}_{\eta,\ell} = \begin{bmatrix} \mu_{\mathrm{r}\ell}\mathbf{A}^{ab}_\ell & \eta^2\mu_{\mathrm{r}\ell}\mathbf{A}^{ab}_\ell & \mathbf{D}^{ab}_{\ell\star} & \mathbf{D}^{ab}_\ell \\ \mu_{\mathrm{r}\ell}\mathbf{A}^{ab}_\ell & \eta^2\mu_{\mathrm{r}\ell}\mathbf{S}^{ab}_\ell & \mathbf{D}^{ab}_\ell & \mathbf{D}^{ab}_\ell \\ \eta^{-p}\mathbf{D}^{ab}_{\ell\star} & \eta^{2-p}\mathbf{D}^{ab}_\ell & \eta^{-p}\mu^{-1}_{\mathrm{r}\ell}(\kappa_\ell L)^2\mathbf{A}^{ab}_\ell & \eta^{-p}\mu^{-1}_{\mathrm{r}\ell}(\kappa_\ell L)^2\mathbf{A}^{ab}_\ell \\ \mathbf{D}^{ab}_\ell & \eta^2\mathbf{D}^{ab}_\ell & \mu^{-1}_{\mathrm{r}\ell}(\kappa_\ell L)^2\mathbf{A}^{ab}_\ell & \mu^{-1}_{\mathrm{r}\ell}(\kappa_\ell L)^2\mathbf{S}^{ab}_\ell \end{bmatrix}, \qquad \widehat{\boldsymbol{Y}}^a_\eta := \begin{Bmatrix} \boldsymbol{f}^a_{\mathrm{s}} \\ \boldsymbol{f}^a_{\mathrm{s}} \\ \eta^{-p}\boldsymbol{g}^a_{\mathrm{s}} \\ \boldsymbol{g}^a_{\mathrm{s}} \end{Bmatrix} \tag{30}$$

(with the exponent p as defined in (28)). The rescaled global operator matrix of problem (29) is well-behaved: all four operators in the diagonal of each diagonal block $\widehat{\boldsymbol{\mathcal{Z}}}^{aa}_{\eta,a}+\widehat{\boldsymbol{\mathcal{Z}}}^{aa}_{\eta,0}$ are of order $O(1)$ in η, and all remaining operators in (29) have leading orders with non-negative powers of η (whereas the original weak problem (16) features $O(\eta^{-1})$ and $O(\eta^{-2})$ blocks).

Remark 1. *Due to the non-symmetric character of the applied row and column scaling, the rescaled form* (29) *of the variational PMCHWT problem is not complex symmetric.*

2.4 Expansion of the rescaled PMCHWT problem.

The asymptotic expansion of the PMCHWT solution is now sought by expanding in powers of η the rescaled weak PMCHWT problem (29).

Expansion of the integral operators. For the vacuum medium, each operator matrix $\widehat{\boldsymbol{\mathcal{Z}}}^{ab}_{\eta,0}$, given by (30) with $\ell=0$, is expanded with the help of $\eta^{-p}(\kappa_0 L)^2 = \eta^{2-p}$ and the operator expansions

$$\mathbf{A}^{ab}_0 = \mathbf{A}^{ab}_{(0)} + O(\eta^2), \qquad \eta^2\mathbf{S}^{ab}_0 = \eta^2\mathbf{A}^{ab}_0 + \mathbf{K}^{ab}_{(0)} + O(\eta^2),$$
$$\mathbf{D}^{ab}_0 = \mathbf{D}^{ab}_{(0)} + O(\eta^2), \qquad \mathbf{D}^{ab}_{0\star} = \eta^2\mathbf{D}^{ab}_{(2)} + O(\eta^4)$$

obtained from using (25) and Lemmas 1, 2 in definitions (12), (15) and (26). This yields

$$\widehat{\boldsymbol{\mathcal{Z}}}^{ab}_{\eta,0} = \widehat{\boldsymbol{\mathcal{Z}}}^{ab}_{(0)} + \eta\widehat{\boldsymbol{\mathcal{Z}}}^{ab}_{(1)} + O(\eta^2)$$

with

$$\widehat{\boldsymbol{\mathcal{Z}}}^{ab}_{(0)} = \begin{bmatrix} \mathbf{A}^{ab}_{(0)} & 0 & 0 & \mathbf{D}^{ab}_{(0)} \\ \mathbf{A}^{ab}_{(0)} & \mathbf{K}^{ab}_{(0)} & \mathbf{D}^{ab}_{(0)} & \mathbf{D}^{ab}_{(0)} \\ 0 & 0 & 0 & 0 \\ \mathbf{D}^{ab}_{(0)} & 0 & 0 & \mathbf{K}^{ab}_{(0)} \end{bmatrix} \quad (a\in\mathcal{C}\cup\mathcal{M}), \quad \widehat{\boldsymbol{\mathcal{Z}}}^{ab}_{(0)} = \begin{bmatrix} \mathbf{A}^{ab}_{(0)} & 0 & 0 & \mathbf{D}^{ab}_{(0)} \\ \mathbf{A}^{ab}_{(0)} & \mathbf{K}^{ab}_{(0)} & \mathbf{D}^{ab}_{(0)} & \mathbf{D}^{ab}_{(0)} \\ \mathbf{D}^{ab}_{(2)} & \mathbf{D}^{ab}_{(0)} & \mathbf{A}^{ab}_{(0)} & \mathbf{A}^{ab}_{(0)} \\ \mathbf{D}^{ab}_{(0)} & 0 & 0 & \mathbf{K}^{ab}_{(0)} \end{bmatrix} \quad (a\in\mathcal{N}).$$

and

$$\widehat{\boldsymbol{\mathcal{Z}}}^{ab}_{(1)} = 0 \quad (a\in\mathcal{C}\cup\mathcal{N}), \qquad \widehat{\boldsymbol{\mathcal{Z}}}^{ab}_{(1)} = \begin{bmatrix} 0 & 0 & 0 & 0 \\ 0 & 0 & 0 & 0 \\ \mathbf{D}^{ab}_{(2)} & \mathbf{D}^{ab}_{(0)} & \mathbf{A}^{ab}_{(0)} & \mathbf{A}^{ab}_{(0)} \\ 0 & 0 & 0 & 0 \end{bmatrix} \quad (a\in\mathcal{M}).$$

Expansions of the rescaled operator matrices associated to each object are obtained in the same way. For HC objects, the kernel expansions (23) lead to the individual operator expansions

$$\begin{aligned} \mathbf{A}^{aa}_a &= \mathbf{A}^{aa}_{\mathrm{C}(0)} + O(\eta^2), & \mathbf{S}^{aa}_a &= \mathbf{A}^{aa}_{\mathrm{C}(0)} + q_a^{-2}\mathbf{K}^{aa}_{\mathrm{C}(0)} + O(\eta^2), \\ \mathbf{D}^{aa}_a &= \mathbf{D}^{aa}_{\mathrm{C}(0)} + O(\eta^2) & \mathbf{D}^{aa}_{a\star} &= \mathbf{D}^{aa}_{\mathrm{C}(0)} - \mathbf{D}^{aa}_{(0)} + O(\eta^2) \end{aligned} \qquad (a\in\mathcal{C})$$

and hence (also recalling that $\kappa_a L = q_a + O(\eta^2)$, see (22))

$$\widehat{\boldsymbol{\mathcal{Z}}}^{aa}_{\eta,a} = \widehat{\boldsymbol{\mathcal{Z}}}^{aa}_{\mathrm{C}(0)} + O(\eta^2), \qquad \widehat{\boldsymbol{\mathcal{Z}}}^{aa}_{\mathrm{C}(0)} = \begin{bmatrix} \mu_{\mathrm{r}a}\mathbf{A}^{aa}_{\mathrm{C}(0)} & 0 & \mathbf{D}^{aa}_{\mathrm{C}(0)} - \mathbf{D}^{aa}_{(0)} & \mathbf{D}^{aa}_{\mathrm{C}(0)} \\ \mu_{\mathrm{r}a}\mathbf{A}^{aa}_{\mathrm{C}(0)} & 0 & \mathbf{D}^{aa}_{\mathrm{C}(0)} & \mathbf{D}^{aa}_{\mathrm{C}(0)} \\ \mathbf{D}^{aa}_{\mathrm{C}(0)} - \mathbf{D}^{aa}_{(0)} & 0 & \mu^{-1}_{\mathrm{r}a}q_a^2\mathbf{A}^{aa}_{\mathrm{C}(0)} & \mu^{-1}_{\mathrm{r}a}q_a^2\mathbf{A}^{aa}_{\mathrm{C}(0)} \\ \mathbf{D}^{aa}_{\mathrm{C}(0)} & 0 & \mu^{-1}_{\mathrm{r}a}q_a^2\mathbf{A}^{aa}_{\mathrm{C}(0)} & \mu^{-1}_{\mathrm{r}a}(q_a^2\mathbf{A}^{aa}_{\mathrm{C}(0)} + \mathbf{K}^{aa}_{\mathrm{C}(0)}) \end{bmatrix}. \tag{31}$$

For NC objects, we have $\kappa_a = q_a\eta$ (see (22)) and use Lemma 2c, so that

$$\begin{aligned} \mathbf{A}^{aa}_a &= \mathbf{A}^{aa}_{(0)} + O(\eta^2), & \eta^2\mathbf{S}^{aa}_a &= q_a^{-2}\mathbf{K}^{aa}_{(0)} + O(\eta^2), \\ \mathbf{D}^{aa}_a &= \mathbf{D}^{aa}_0 + O(\eta^2), & \mathbf{D}^{aa}_{a\star} &= q_a^2\eta^2\mathbf{D}^{aa}_{(2)} + O(\eta^4) \end{aligned} \qquad (a\in\mathcal{N})$$

(where, as stressed earlier in Sec. 2.1, operator-valued coefficients such as $\mathbf{A}^{aa}_{(p)}$ are defined as for the vacuum), from which we obtain

$$\widehat{\boldsymbol{\mathcal{Z}}}^{aa}_{\eta,a} = \widehat{\boldsymbol{\mathcal{Z}}}^{aa}_{\mathrm{N}(0)} + O(\eta^2), \qquad \widehat{\boldsymbol{\mathcal{Z}}}^{aa}_{\mathrm{N}(0)} = \begin{bmatrix} \mu_{ra}\mathbf{A}^{aa}_{(0)} & 0 & 0 & \mathbf{D}^{aa}_{(0)} \\ \mu_{ra}\mathbf{A}^{aa}_{(0)} & \mu_{ra}q_a^{-2}\mathbf{K}^{aa}_{(0)} & \mathbf{D}^{aa}_{(0)} & \mathbf{D}^{aa}_{(0)} \\ q_a^2\mathbf{D}^{aa}_{(2)} & \mathbf{D}^{aa}_{(0)} & \mu_{ra}^{-1}q_a^2\mathbf{A}^{aa}_{(0)} & \mu_{ra}^{-1}q_a^2\mathbf{A}^{aa}_{(0)} \\ \mathbf{D}^{aa}_{(0)} & 0 & 0 & \mu_{ra}^{-1}\mathbf{K}^{aa}_{(0)} \end{bmatrix}.$$

Finally, for MC objects, we have $(\kappa_a L)^2 = q_a^2\eta + 2q_a^4 q_a'\eta^2 + O(\eta^3)$ (see (22)) and

$$\begin{aligned} \mathbf{A}^{aa}_{a} &= \mathbf{A}^{aa}_{(0)} + \eta q_a^2\mathbf{A}^{aa}_{(2)} + \eta^{3/2}q_a^3\mathbf{A}^{aa}_{(3)} + O(\eta^2), \\ \eta^2\mathbf{S}^{aa}_{a} &= \eta q_a^{-2}\mathbf{K}^{aa}_{(0)} + O(\eta^2), \\ (\kappa_a L)^2\mathbf{S}^{aa}_{a} &= \mathbf{K}^{aa}_{(0)} + \eta q_a^2(\mathbf{K}^{aa}_{(2)} + \mathbf{A}^{aa}_{(0)}) + \eta^{3/2}q_a^3(\mathbf{K}^{aa}_{(3)} + \mathbf{A}^{aa}_{(1)}) + O(\eta^2), \qquad (a\in\mathcal{M}) \\ \mathbf{D}^{aa}_{a} &= \mathbf{D}^{aa}_{(0)} + \eta q_a^2\mathbf{D}^{aa}_{(2)} + \eta^{3/2}q_a^3\mathbf{D}^{aa}_{(3)} + \eta^2 q_a^4\big(\mathbf{D}^{aa}_{(4)} + 2q_a'\mathbf{D}^{aa}_{(2)}\big) + O(\eta^{5/2}), \\ \mathbf{D}^{aa}_{a\star} &= \eta q_a^2\mathbf{D}^{aa}_{(2)} + \eta^2 q_a^4\big(\mathbf{D}^{aa}_{(4)} + 2q_a'\mathbf{D}^{aa}_{(2)}\big) + \eta^{5/2}q_a^5\mathbf{D}^{aa}_{(5)} + O(\eta^3), \end{aligned}$$

(again in terms of the vacuum-based operator coefficients $\mathbf{A}^{aa}_{(0)}$ etc.), leading to the operator matrix expansion

$$\widehat{\boldsymbol{\mathcal{Z}}}^{aa}_{\mathrm{M}\eta,} = \widehat{\boldsymbol{\mathcal{Z}}}^{aa}_{\mathrm{M}(0)} + \eta\widehat{\boldsymbol{\mathcal{Z}}}^{aa}_{\mathrm{M}(1)} + \eta^{3/2}\widehat{\boldsymbol{\mathcal{Z}}}^{aa}_{\mathrm{M}(3/2)} + O(\eta^2)$$

with

$$\widehat{\boldsymbol{\mathcal{Z}}}^{aa}_{\mathrm{M}(0)} = \begin{bmatrix} \mu_{ra}\mathbf{A}^{aa}_{(0)} & 0 & 0 & \mathbf{D}^{aa}_{(0)} \\ \mu_{ra}\mathbf{A}^{aa}_{(0)} & 0 & \mathbf{D}^{aa}_{(0)} & \mathbf{D}^{aa}_{(0)} \\ q_a^2\mathbf{D}^{aa}_{(2)} & 0 & \mu_{ra}^{-1}q_a^2\mathbf{A}^{aa}_{(0)} & \mu_{ra}^{-1}q_a^2\mathbf{A}^{aa}_{(0)} \\ \mathbf{D}^{aa}_{(0)} & 0 & 0 & \mu_{ra}^{-1}\mathbf{K}^{aa}_{(0)} \end{bmatrix},$$

$$\widehat{\boldsymbol{\mathcal{Z}}}^{aa}_{\mathrm{M}(1)} = \begin{bmatrix} \mu_{ra}q_a^2\mathbf{A}^{aa}_{(2)} & 0 & q_a^2\mathbf{D}^{aa}_{(2)} & q_a^2\mathbf{D}^{aa}_{(2)} \\ \mu_{ra}q_a^2\mathbf{A}^{aa}_{(2)} & \mu_{ra}q_a^{-2}\mathbf{K}^{aa}_{(0)} & q_a^2\mathbf{D}^{aa}_{(2)} & q_a^2\mathbf{D}^{aa}_{(2)} \\ q_a^4(\mathbf{D}^{aa}_{(4)} + 2q_a'\mathbf{D}^{aa}_{(2)}) & \mathbf{D}^{aa}_{(0)} & \mu_{ra}^{-1}q_a^4(\mathbf{A}^{aa}_{(2)} + 2q_a'\mathbf{A}^{aa}_{(0)}) & \mu_{ra}^{-1}q_a^4(\mathbf{A}^{aa}_{(2)} + 2q_a'\mathbf{A}^{aa}_{(0)}) \\ q_a^2\mathbf{D}^{aa}_{(2)} & 0 & \mu_{ra}^{-1}q_a^2\mathbf{A}^{aa}_{(0)} & \mu_{ra}^{-1}q_a^2(\mathbf{A}^{aa}_{(0)} + \mathbf{K}^{aa}_{(2)}) \end{bmatrix},$$

$$\widehat{\boldsymbol{\mathcal{Z}}}^{aa}_{\mathrm{M}(3/2)} = \begin{bmatrix} \mu_{ra}q_a^3\mathbf{A}^{aa}_{(3)} & 0 & 0 & q_a^3\mathbf{D}^{aa}_{(3)} \\ \mu_{ra}q_a^3\mathbf{A}^{aa}_{(3)} & 0 & q_a^3\mathbf{D}^{aa}_{(3)} & q_a^3\mathbf{D}^{aa}_{(3)} \\ q_a^5\mathbf{D}^{aa}_{(5)} & 0 & \mu_{ra}^{-1}q_a^5\mathbf{A}^{aa}_{(3)} & \mu_{ra}^{-1}q_a^5\mathbf{A}^{aa}_{(3)} \\ q_a^3\mathbf{D}^{aa}_{(3)} & 0 & 0 & \mu_{ra}^{-1}q_a^3(\mathbf{A}^{aa}_{(1)} + \mathbf{K}^{aa}_{(3)}) \end{bmatrix}$$

after invoking Lemma 2c,d, which in particular yields $\widehat{\boldsymbol{\mathcal{Z}}}^{aa}_{\mathrm{M}(1/2)} = 0$.

Expansion of the right-hand side. Applying expansions (25) to the source terms given by (13) and using Lemma 1, we find

$$\boldsymbol{f}^a_{\mathrm{s}} = \boldsymbol{f}^a_{\mathrm{s}(0)} + O(\eta^2), \quad \big\langle \boldsymbol{\phi}_{\mathrm{L}}, \boldsymbol{g}^a_{\mathrm{s}} \big\rangle_{\times} = \eta^2 \big\langle \boldsymbol{\phi}_{\mathrm{L}}, \boldsymbol{g}^a_{\mathrm{s}(2)} \big\rangle_{\times} + O(\eta^4), \quad \big\langle \boldsymbol{\phi}_{\mathrm{T}}, \boldsymbol{g}^a_{\mathrm{s}} \big\rangle_{\times} = \big\langle \boldsymbol{\phi}_{\mathrm{T}}, \boldsymbol{g}^a_{\mathrm{s}(0)} \big\rangle_{\times} + O(\eta^2),$$

so that the rescaled right-hand side $\widehat{\boldsymbol{Y}}^a_\eta$ given by (30) has the expansion

$$\widehat{\boldsymbol{Y}}^a_\eta = \widehat{\boldsymbol{Y}}^a_{(0)} + \eta\widehat{\boldsymbol{Y}}^a_{(1)} + O(\eta^2)$$

with

$$\begin{aligned} \widehat{\boldsymbol{Y}}^a_{(0)} &= \big\{ \boldsymbol{f}^a_{\mathrm{s}(0)}, \boldsymbol{f}^a_{\mathrm{s}(0)}, 0, \boldsymbol{g}^a_{\mathrm{s}(0)} \big\}^{\mathrm{T}} \qquad (a\in\mathcal{C}\cup\mathcal{M}), \\ &= \big\{ \boldsymbol{f}^a_{\mathrm{s}(0)}, \boldsymbol{f}^a_{\mathrm{s}(0)}, \boldsymbol{g}^a_{\mathrm{s}(2)}, \boldsymbol{g}^a_{\mathrm{s}(0)} \big\}^{\mathrm{T}} \qquad (a\in\mathcal{N}), \end{aligned} \qquad \begin{aligned} \widehat{\boldsymbol{Y}}^a_{(1)} &= \big\{ 0, 0, 0, 0 \big\}^{\mathrm{T}} \qquad (a\in\mathcal{C}\cup\mathcal{N}), \\ &= \big\{ 0, 0, \boldsymbol{g}^a_{\mathrm{s}(2)}, 0 \big\}^{\mathrm{T}} \qquad (a\in\mathcal{M}) \end{aligned}$$

Expansion of the current densities. Let the rescaled PMCHWT problem (29) be written in compact form as

$$\text{Find } \widehat{\mathbb{X}}_\eta \in \mathbb{V}, \qquad \big\langle \widetilde{\mathbb{X}},\, \widehat{\mathbb{Z}}_\eta \widehat{\mathbb{X}}_\eta \big\rangle_\times = \big\langle \widetilde{\mathbb{X}},\, \widehat{\mathbb{Y}}_\eta \big\rangle_\times \quad \text{for all } \widetilde{\mathbb{X}} \in \mathbb{V} \tag{32}$$

where $\big\langle \cdot, \cdot \big\rangle_\times$ sums all individual twisted products. The $4M \times 4M$ operator matrix $\widehat{\mathbb{Z}}_\eta$ and $4M$-vector right-hand side $\widehat{\mathbb{Y}}_\eta$, which can readily be identified from the blockwise formulation of (29), have thus been found to have expansions of the form

$$\widehat{\mathbb{Z}}_\eta = \widehat{\mathbb{Z}}_0 + \eta \widehat{\mathbb{Z}}_1 + \eta^{3/2} \widehat{\mathbb{Z}}_{3/2} + O(\eta^2), \qquad \widehat{\mathbb{Y}}_\eta = \widehat{\mathbb{Y}}_0 + \eta \widehat{\mathbb{Y}}_1 + O(\eta^2) \tag{33}$$

where the coefficients $\widehat{\mathbb{Z}}_p$ and $\widehat{\mathbb{Y}}_p$ are also found by identification. Making the natural ansatz

$$\widehat{\mathbb{X}}_\eta = \widehat{\mathbb{X}}_0 + \eta \widehat{\mathbb{X}}_1 + \eta^{3/2} \widehat{\mathbb{X}}_{3/2} + O(\eta^2) \tag{34}$$

for the rescaled solution, we insert (33) and (34) in (32) and expand the resulting equality to order $O(\eta^{3/2})$. The coefficients $\widehat{\mathbb{X}}_m$ are as a result sequentially governed by the integral problems

$$\begin{aligned}
&\text{(a)} && \big\langle \widetilde{\mathbb{X}},\, \widehat{\mathbb{Z}}_0 \widehat{\mathbb{X}}_0 \big\rangle_\times = \big\langle \widetilde{\mathbb{X}},\, \widehat{\mathbb{Y}}_0 \big\rangle_\times && \text{for all } \widetilde{\mathbb{X}} \in \mathbb{V} \\
&\text{(b)} && \big\langle \widetilde{\mathbb{X}},\, \widehat{\mathbb{Z}}_0 \widehat{\mathbb{X}}_1 \big\rangle_\times = \big\langle \widetilde{\mathbb{X}},\, \widehat{\mathbb{Y}}_1 - \widehat{\mathbb{Z}}_1 \widehat{\mathbb{X}}_0 \big\rangle_\times && \text{for all } \widetilde{\mathbb{X}} \in \mathbb{V} \\
&\text{(c)} && \big\langle \widetilde{\mathbb{X}},\, \widehat{\mathbb{Z}}_0 \widehat{\mathbb{X}}_{3/2} \big\rangle_\times = -\big\langle \widetilde{\mathbb{X}},\, \widehat{\mathbb{Z}}_{3/2} \widehat{\mathbb{X}}_0 \big\rangle_\times && \text{for all } \widetilde{\mathbb{X}} \in \mathbb{V}
\end{aligned} \tag{35}$$

This results, in view of the adopted scaling $\boldsymbol{J}^a_{\mathrm{T}} = \eta^2 \widehat{\boldsymbol{J}}^a_{\mathrm{T}}$, in the original surface current densities on each surface Γ_a having the expansions

$$\begin{aligned}
\boldsymbol{J}^a_{\mathrm{L}} &= \quad \widehat{\boldsymbol{J}}^a_{\mathrm{L}(0)} + \eta \widehat{\boldsymbol{J}}^a_{\mathrm{L}(1)} + \eta^{3/2} \widehat{\boldsymbol{J}}^a_{\mathrm{L}(3/2)} + O(\eta^2) \\
\boldsymbol{J}^a_{\mathrm{T}} &= \eta^2 \big(\widehat{\boldsymbol{J}}^a_{\mathrm{T}(0)} + \eta \widehat{\boldsymbol{J}}^a_{\mathrm{T}(1)} + \eta^{3/2} \widehat{\boldsymbol{J}}^a_{\mathrm{T}(3/2)} + O(\eta^2) \big) \\
\boldsymbol{M}^a_{\mathrm{L}} &= \quad \widehat{\boldsymbol{M}}^a_{\mathrm{L}(0)} + \eta \widehat{\boldsymbol{M}}^a_{\mathrm{L}(1)} + \eta^{3/2} \widehat{\boldsymbol{M}}^a_{\mathrm{L}(3/2)} + O(\eta^2) \\
\boldsymbol{M}^a_{\mathrm{T}} &= \quad \widehat{\boldsymbol{M}}^a_{\mathrm{T}(0)} + \eta \widehat{\boldsymbol{M}}^a_{\mathrm{T}(1)} + \eta^{3/2} \widehat{\boldsymbol{M}}^a_{\mathrm{T}(3/2)} + O(\eta^2)
\end{aligned} \tag{36}$$

The expansion of the PMCHWT problem and solution derived in this section contains as a special case the expansion established in [6] for a single HC object, once correspondences between dimensionless parameters recalled in the beginning of this section are taken into account. The small-γ expansion of [6] was given a rigorous justification, whereas here we limit ourselves to a formal expansion. We expect that straightforward extensions of the arguments used in [6] would allow to justify our present treatment of more-complex configurations, and elected to forgo this step to avoid excessive length for this article.

Remark 2. *We observe in passing that the* 2×2 *lower diagonal sub-block of the operator matrix* $\widehat{\boldsymbol{\mathcal{Z}}}^{aa}_{C(0)}$ *for a HC body is proportional to* $q_a^2 = -\mu_{ra}\xi_a^2 = O(L^2/\delta_a^2)$ *(where* δ_a *is the skin depth for the HC material). Although* ξ_a *is treated as fixed,* ξ_a^2 *may for thin bodies take* $O(10^2 - 10^4)$ *values if* L *is set to some characteristic object diameter, high enough to deteriorate the condition number of* $\widehat{\boldsymbol{\mathcal{Z}}}^{aa}_{C(0)}$*. This potential problem may be avoided by rescaling* $\boldsymbol{M}^a$ *through* $\boldsymbol{M}^a = q_a^2 \widehat{\boldsymbol{M}^a}$*.*

2.5 Expansion of the field perturbations and impedance variation.

The Helmholtz-Hodge decomposition and the asymptotic approximations of the surface current densities are now used in the Stratton-Chu representation formulas (10) of $\boldsymbol{E}$ and (11) of $\boldsymbol{H}$. This yields the asymptotic approximations

$$\boldsymbol{E} = \eta \big(\boldsymbol{E}_{(0)} + \eta \boldsymbol{E}_{(1)} + \eta^{3/2} \boldsymbol{E}_{(3/2)} + O(\eta^2) \big) \tag{37a}$$

$$\boldsymbol{H} = \quad \boldsymbol{H}_{(0)} + \eta \boldsymbol{H}_{(1)} + \eta^{3/2} \boldsymbol{H}_{(3/2)} + O(\eta^2) \tag{37b}$$

of the electromagnetic fields in the vacuum and in each object, where for $p = 0, 1, \frac{3}{2}$ we have

$$\boldsymbol{E}_{(p)} = \mathrm{i}\sigma_{\mathrm{ref}}^{-1} L^{-2} \Big(\boldsymbol{\Phi}_{(0)}[\boldsymbol{J}_{\mathrm{s}}] \delta_{p0} - \sum_{a=1}^{M} \big[\boldsymbol{\mathcal{A}}^a_{(0)} \widehat{\boldsymbol{J}}^a_{\mathrm{L}(p)} + \boldsymbol{\mathcal{K}}^a_{(0)} \widehat{\boldsymbol{J}}^a_{\mathrm{T}(p)} + \boldsymbol{\mathcal{D}}^a_{(0)} \big(\widehat{\boldsymbol{M}}^a_{\mathrm{L}(p)} + \widehat{\boldsymbol{M}}^a_{\mathrm{T}(p)} \big) \big] \Big),$$

$$\boldsymbol{H}_{(p)} = \mathbf{rot}\, \boldsymbol{\Phi}_{(0)}[\boldsymbol{J}_{\mathrm{s}}] \delta_{p0} - L^{-1} \sum_{a=1}^{M} \big[\boldsymbol{\mathcal{D}}^a_{(0)} \widehat{\boldsymbol{J}}^a_{\mathrm{L}(p)} + \boldsymbol{\mathcal{K}}^a_{(0)} \widehat{\boldsymbol{M}}^a_{\mathrm{T}(p)} \big]$$

in the vacuum Ω_0,

$$\begin{aligned}
\boldsymbol{E}_{(p)} &= \mathrm{i}\sigma_{\mathrm{ref}}^{-1}L^{-2}\big(\mu_{\mathrm{ra}}\boldsymbol{\mathcal{A}}^a_{\mathrm{C}(0)}\widehat{\boldsymbol{J}}^a_{\mathrm{L}(p)} + \boldsymbol{\mathcal{D}}^a_{\mathrm{C}(0)}\big[\widehat{\boldsymbol{M}}^a_{\mathrm{L}(p)} + \widehat{\boldsymbol{M}}^a_{\mathrm{T}(p)}\big]\big),\\
\boldsymbol{H}_{(p)} &= L^{-1}\big(\boldsymbol{\mathcal{D}}^a_{\mathrm{C}(0)}\widehat{\boldsymbol{J}}^a_{\mathrm{L}(p)} + \mu_{\mathrm{ra}}^{-1}q_a^2\boldsymbol{\mathcal{A}}^a_{\mathrm{C}(0)}\widehat{\boldsymbol{M}}^a_{\mathrm{L}(p)} + \mu_{\mathrm{ra}}^{-1}\big[q_a^2\boldsymbol{\mathcal{A}}^a_{\mathrm{C}(0)} + \boldsymbol{\mathcal{K}}^a_{\mathrm{C}(0)}\big]\widehat{\boldsymbol{M}}^a_{\mathrm{T}(p)}\big)
\end{aligned} \qquad (a\in\mathcal{C})$$

in a HC body Ω_a,

$$\begin{aligned}
\boldsymbol{E}_{(p)} &= \mathrm{i}\sigma_{\mathrm{ref}}^{-1}L^{-2}\Big(\mu_{\mathrm{ra}}\boldsymbol{\mathcal{A}}^a_{(0)}\widehat{\boldsymbol{J}}^a_{\mathrm{L}(p)} + \mu_{\mathrm{ra}}\boldsymbol{\mathcal{K}}^a_{(0)}\widehat{\boldsymbol{J}}^a_{\mathrm{T}(p)} + \boldsymbol{\mathcal{D}}^a_{(0)}\widehat{\boldsymbol{M}}^a_{\mathrm{L}(p)} + \boldsymbol{\mathcal{D}}^a_{(0)}\widehat{\boldsymbol{M}}^a_{\mathrm{T}(p)}\Big)\\
\boldsymbol{H}_{(p)} &= L^{-1}\big(\boldsymbol{\mathcal{D}}^a_{(0)}\widehat{\boldsymbol{J}}^a_{\mathrm{L}(p)} + \mu_{\mathrm{ra}}^{-1}\boldsymbol{\mathcal{K}}^a_{(0)}\widehat{\boldsymbol{M}}^a_{\mathrm{T}(p)}\big)
\end{aligned} \qquad (a\in\mathcal{N})$$

in a NC body Ω_a, and

$$\begin{aligned}
\boldsymbol{E}_{(p)} &= \mathrm{i}\sigma_{\mathrm{ref}}^{-1}L^{-2}\Big(\mu_{\mathrm{ra}}\boldsymbol{\mathcal{A}}^a_{(0)}\widehat{\boldsymbol{J}}^a_{\mathrm{L}(p)} + \boldsymbol{\mathcal{D}}^a_{(0)}\big(\widehat{\boldsymbol{M}}^a_{\mathrm{L}(p)} + \widehat{\boldsymbol{M}}^a_{\mathrm{T}(p)}\big) + \delta_{p1}\,\mu_{\mathrm{ra}}q_a^{-2}\,\boldsymbol{\mathcal{K}}^a_{(0)}\widehat{\boldsymbol{J}}^a_{\mathrm{T}(0)}\\
&\qquad + (1-\delta_{p0})\,q_a^{2p}\big[\mu_{\mathrm{ra}}\boldsymbol{\mathcal{A}}^a_{(2p)}\widehat{\boldsymbol{J}}^a_{\mathrm{L}(0)} + \boldsymbol{\mathcal{D}}^a_{(2p)}\big(\widehat{\boldsymbol{M}}^a_{\mathrm{L}(0)} + \widehat{\boldsymbol{M}}^a_{\mathrm{T}(0)}\big)\big]\Big)\\
\boldsymbol{H}_{(p)} &= L^{-1}\Big(\boldsymbol{\mathcal{D}}^a_{(0)}\widehat{\boldsymbol{J}}^a_{\mathrm{L}(p)} + \mu_{\mathrm{ra}}^{-1}\boldsymbol{\mathcal{K}}^a_{(0)}\widehat{\boldsymbol{M}}^a_{\mathrm{T}(p)} + \delta_{p1}\,\mu_{\mathrm{ra}}^{-1}q_a^2\boldsymbol{\mathcal{A}}^a_{(0)}\widehat{\boldsymbol{M}}^a_{\mathrm{L}(0)}\\
&\qquad + (1-\delta_{p0})\,\big(q_a^{2p}\,\boldsymbol{\mathcal{D}}^a_{(2p)}\widehat{\boldsymbol{J}}^a_{\mathrm{L}(0)} + \mu_{\mathrm{ra}}^{-1}q_a^{2p}\big[\boldsymbol{\mathcal{K}}^a_{(2p)} + \boldsymbol{\mathcal{A}}^a_{(2p-2)}\big]\widehat{\boldsymbol{M}}^a_{\mathrm{T}(0)}\big)\Big)
\end{aligned} \qquad (a\in\mathcal{M})$$

in a MC body Ω_a. In the above formulas for $\boldsymbol{E}_{(p)}$ and $\boldsymbol{H}_{(p)}$, the notations $\boldsymbol{\mathcal{A}}^a_{\mathrm{C}(0)}$, $\boldsymbol{\mathcal{D}}^a_{\mathrm{C}(0)}$, $\boldsymbol{\mathcal{K}}^a_{\mathrm{C}(0)}$ respectively stand for the potentials $\boldsymbol{\mathcal{A}}^a_a$, $\boldsymbol{\mathcal{D}}^a_a$, $\boldsymbol{\mathcal{K}}^a_a$ with $G(\cdot;\kappa_a)$ replaced with $G^{\mathrm{C}}_{(0)}$ (case $a\in\mathcal{C}$), while $\boldsymbol{\mathcal{A}}^a_{(m)}$, $\boldsymbol{\mathcal{D}}^a_{(m)}$, $\boldsymbol{\mathcal{K}}^a_{(m)}$ are the respective potentials $\boldsymbol{\mathcal{A}}^a_0$, $\boldsymbol{\mathcal{D}}^a_0$, $\boldsymbol{\mathcal{K}}^a_0$ with $G(\cdot;\kappa_0)$ replaced with $G_m(\cdot)$ (all other cases); moreover, δ_{p0} and δ_{p1} are Kronecker symbols.

The expansion of the impedance variation is found in a similar way, and we have

$$\Delta Z = \eta\big(\Delta Z_{(0)} + \eta\Delta Z_{(1)} + \eta^{3/2}\Delta Z_{(3/2)} + O(\eta^2)\big) \tag{38}$$

with

$$\Delta Z_{(p)} = \frac{\mathrm{i}}{\sigma_{\mathrm{ref}}L^2I^2}\sum_a\Big(\big\langle\widehat{\boldsymbol{J}}^a_{\mathrm{L}(p)},\,\boldsymbol{f}^a_{\mathrm{s}(0)}\big\rangle^a_\times + \big\langle\widehat{\boldsymbol{M}}^a_{\mathrm{T}(p)},\,\boldsymbol{g}^a_{\mathrm{s}(0)}\big\rangle^a_\times\Big) \qquad (p=0,1,\tfrac{3}{2})$$

Expansions (37a,b) and (38), together with their various components (whose details are given earlier in this section) and expansions (36) of the surface current densities, constitute the main theoretical results of this work. The detail of those ingredients have useful implications on the computational implementation of the proposed asymptotic expansions (Section 2.6) and on special cases and extensions (Section 3).

2.6 Blockwise solution. The operator matrices $\widehat{\boldsymbol{\mathcal{Z}}}^{ab}_{(0)}$ and $\widehat{\boldsymbol{\mathcal{Z}}}^{aa}_{\eta(0)}$ each feature some null operators, which results in the global operator matrix $\widehat{\mathbb{Z}}_{(0)}$ also having some null entries. A close examination of the population of $\widehat{\mathbb{Z}}_{(0)}$ shows that any system of the form $\widehat{\mathbb{Z}}_{(0)}\widehat{\mathbb{X}} = \widehat{\mathbb{Y}}$ can be solved blockwise in three stages:

- Stage 1: solve for $\widehat{\mathbb{X}}' := \big\{(\widehat{\boldsymbol{J}}^a_{\mathrm{L}},\widehat{\boldsymbol{M}}^a_{\mathrm{L}},\widehat{\boldsymbol{M}}^a_{\mathrm{T}})_{a\in\mathcal{C}},\,(\widehat{\boldsymbol{J}}^a_{\mathrm{L}},\widehat{\boldsymbol{M}}^a_{\mathrm{T}})_{a\in\mathcal{N}\cup\mathcal{M}}\big\}$, using the equations yielded by the corresponding subset of test functions $\widetilde{\mathbb{X}}' := \big\{(\widetilde{\boldsymbol{J}}^a_{\mathrm{L}},\widetilde{\boldsymbol{M}}^a_{\mathrm{L}},\widetilde{\boldsymbol{M}}^a_{\mathrm{T}})_{a\in\mathcal{C}},\,(\widetilde{\boldsymbol{J}}^a_{\mathrm{L}},\widetilde{\boldsymbol{M}}^a_{\mathrm{T}})_{a\in\mathcal{N}\cup\mathcal{M}}\big\}$. This can be symbolized as $\widehat{\mathbb{Z}}'_{(0)}\widehat{\mathbb{X}}' = \widehat{\mathbb{Y}}'$, where $\widehat{\mathbb{Z}}'_{(0)}$ and $\widehat{\mathbb{Y}}'$ are the appropriate parts of the operator matrix and right-hand side.
- Stage 2: solve for $\widehat{\mathbb{X}}'' := \big\{(\widehat{\boldsymbol{J}}^a_{\mathrm{T}})_{a\in\mathcal{C}},\,(\widehat{\boldsymbol{J}}^a_{\mathrm{T}},\widehat{\boldsymbol{M}}^a_{\mathrm{L}})_{a\in\mathcal{N}},\,(\widehat{\boldsymbol{M}}^a_{\mathrm{L}})_{a\in\mathcal{M}}\big\}$, using the equations yielded by the corresponding subset of test functions $\widetilde{\mathbb{X}}'' := \big\{(\widetilde{\boldsymbol{J}}^a_{\mathrm{T}})_{a\in\mathcal{C}},\,(\widetilde{\boldsymbol{J}}^a_{\mathrm{T}},\widetilde{\boldsymbol{M}}^a_{\mathrm{L}})_{a\in\mathcal{N}},\,(\widetilde{\boldsymbol{M}}^a_{\mathrm{L}})_{a\in\mathcal{M}}\big\}$.
- Stage 3: solve for $\widehat{\mathbb{X}}''' := \big\{(\widehat{\boldsymbol{J}}^a_{\mathrm{T}})_{a\in\mathcal{M}}\big\}$, using the equations yielded by the corresponding subset of test functions $\widetilde{\mathbb{X}}''' := \big\{(\widetilde{\boldsymbol{J}}^a_{\mathrm{T}})_{a\in\mathcal{M}}\big\}$.

Those stages can be applied to each of the sequential integral problems (35). Moreover, stage 1 suffices for obtaining the leading-order asymptotic approximations of ΔZ, of $\boldsymbol{H}$ everywhere, and of $\boldsymbol{E}$ in the HC bodies, allowing computational savings. For example, if $|\mathcal{C}| = |\mathcal{N}| = |\mathcal{M}|$, solving a stage-1 system using a traditional direct method requires only $(7/12)^3 \approx 0.2$ times the computational work for the full system solved at once. Moreover, the operator matrix $\widehat{\mathbb{Z}}'_{(0)}$ governing the stage-1 systems is symmetric; more precisely, its diagonal operator blocks associated with HC bodies (if any) are complex symmetric, and all other operator blocks are real symmetric. These properties allow reductions in both memory requirements and solution time for stage-1 systems.

3 Special cases and extensions.

The special case where no MC bodies are present (Section 3.1) leads to much simpler asymptotic approximations; moreover, MC bodies are found to be treatable as NC for obtaining most of the leading-order aproximations (Section 3.2). Then, each object having until now been assumed to be homogeneous and simply-connected, we extend in Sections 3.3 and 3.4 the asymptotic approximation results of Section 2 to bi-material and multiply-connected objects, respectively.

3.1 No moderately-conducting body. In the absence of MC bodies, we have $\widehat{\mathbb{Z}}_1 = \widehat{\mathbb{Z}}_{3/2} = 0$ and $\widehat{\mathbb{Y}}_1 = 0$, the current density expansion reduces to

$$\widehat{\mathbb{X}}_\eta = \widehat{\mathbb{X}}_0 + O(\eta^2) \qquad \text{with } \widehat{\mathbb{X}}_0 \text{ solving (35a)},$$

and stage 3 in the blockwise solution approach becomes void. This of course includes the pure eddy-current case (where $\mathcal{C} = \{1, \ldots, M\}$) previously addressed in [6]. The various quantities of interest have as a result the simpler expansions

$$\boldsymbol{E} = \eta\big(\eta \boldsymbol{E}_{(0)} + O(\eta^2)\big), \qquad \boldsymbol{H} = \boldsymbol{H}_{(0)} + O(\eta^2), \qquad \Delta Z = \eta\big(\Delta Z_{(0)} + O(\eta^2)\big),$$

with $\boldsymbol{E}_{(0)}$, $\boldsymbol{H}_{(0)}$ and $\Delta Z_{(0)}$ still as given for (37a,b) and (38).

3.2 Approximating MC media by NC media. A closer examination of the three-stage procedure applied to the leading-order surface currents $\widehat{\mathbb{X}}_{(0)}$ reveals that the operator submatrix $\widehat{\mathbb{Z}}'_{(0)}$ does not depend on the conductivity coefficients ξ_a of the MC bodies, if any. Treating the latter as NC hence produces the same $\widehat{\mathbb{Z}}'_{(0)}$, and therefore the correct leading-order contribution $\widehat{\mathbb{X}}'_{(0)}$ to the global scattering solution.

Subsequently, observing that the approximations (37a,b) of $\boldsymbol{E}$, $\boldsymbol{H}$ and (38) of ΔZ for $a \in \mathcal{M}$ depend on ξ_a only through the current density approximations, we find that this procedure yields the correct leading approximation of $\boldsymbol{H}$ everywhere, of $\boldsymbol{E}$ in all HC objects, and of ΔZ.

3.3 Bi-material objects. In this section, we extend the previous asymptotic-approximation treatment to the case where some of the bodies are bi-material. Such bodies are assumed to consist of a HC core occupying the domain D_α and surrounded with a NC or MC material occupying the domain D_a (Fig. 2). We denote by Γ_α the core boundary and Γ_a the interface connecting D_a to Ω_0, so that we have $\partial D_a = \Gamma_a \cup \Gamma_\alpha$ and $\partial D_\alpha = \Gamma_\alpha$; the surfaces Γ_a, Γ_α are both assumed to be simply-connected. The object $\Omega_a = D_a \cup D_\alpha$ can be viewed as a composite body embedded in vacuum, and we let the list $\mathcal{B}$ collect the B indices of all composite bodies (we thus now have $\{1, \ldots, M\} = \mathcal{C} \cup \mathcal{N} \cup \mathcal{M} \cup \mathcal{B}$). To each $a \in \mathcal{B}$ is associated the label $\alpha = \alpha(a)$ of the core D_α and its interface Γ_α (with $M+1 \le \alpha \le M+B$).

The embedded surfaces Γ_α carry additional unknown current densities $\boldsymbol{J}^\alpha, \boldsymbol{M}^\alpha$. With the foregoing notations, the Stratton-Chu representation formulas for the electric field in D_a and D_α read

$$\begin{aligned} \boldsymbol{E} &= \mathrm{i}\mu_0\omega \Big\{ \mu_{ra} \boldsymbol{\mathcal{S}}_a^a[\boldsymbol{J}^a] + \boldsymbol{\mathcal{D}}_a^a[\boldsymbol{M}^a] - \mu_{ra} \boldsymbol{\mathcal{S}}_a^\alpha[\boldsymbol{J}^\alpha] - \boldsymbol{\mathcal{D}}_a^\alpha[\boldsymbol{M}^\alpha] \Big\} && \text{in } D_a, \\ \boldsymbol{E} &= \mathrm{i}\mu_0\omega \big(\mu_{r\alpha} \boldsymbol{\mathcal{S}}_\alpha^\alpha[\boldsymbol{J}^b] + \boldsymbol{\mathcal{D}}_\alpha^\alpha[\boldsymbol{M}^b] \big) && \text{in } D_\alpha. \end{aligned}$$

(with $\alpha = \alpha(a)$). A suitable adaptation of the procedure leading to (14) produces for the PMCHWT integral problem the weak formulation

$$\begin{aligned} &\sum_{a\in\mathcal{B}} \Big(\langle \widetilde{\boldsymbol{X}}^\alpha, (\boldsymbol{\mathcal{Z}}_\alpha^{\alpha\alpha} + \boldsymbol{\mathcal{Z}}_a^{\alpha\alpha}) \boldsymbol{X}^\alpha \rangle_\times^\alpha + \langle \widetilde{\boldsymbol{X}}^\alpha, \boldsymbol{\mathcal{Z}}_a^{\alpha a} \boldsymbol{X}^a \rangle_\times^\alpha + \langle \widetilde{\boldsymbol{X}}^a, \boldsymbol{\mathcal{Z}}_a^{a\alpha} \boldsymbol{X}^\alpha \rangle_\times^\alpha \Big) \\ &\quad + \sum_{a=1}^M \sum_{b=1}^M \langle \widetilde{\boldsymbol{X}}^a, (\boldsymbol{\mathcal{Z}}_a^{ab} \delta_{ab} + \boldsymbol{\mathcal{Z}}_0^{ab}) \boldsymbol{X}^b \rangle_\times^a = \sum_{a=1}^M \langle \widetilde{\boldsymbol{X}}^a, \boldsymbol{Y}^a \rangle_\times^a \qquad \text{for all } \widetilde{\mathbb{X}} = \big(\widetilde{\boldsymbol{X}}^1, \ldots, \widetilde{\boldsymbol{X}}^M\big) \in \mathbb{V}, \quad (39) \end{aligned}$$

instead of (16), the global function space being redefined as $\mathbb{V} := \boldsymbol{\mathcal{V}}^1 \times \boldsymbol{\mathcal{V}}^1 \times \ldots \times \boldsymbol{\mathcal{V}}^{M+B} \times \boldsymbol{\mathcal{V}}^{M+B}$ in order to include the additional unknowns on the bi-material interfaces Γ_α and the corresponding test functions. All terms not involving a bimaterial interface (i.e. an index $\alpha = \alpha(a)$) can be rescaled as previously.

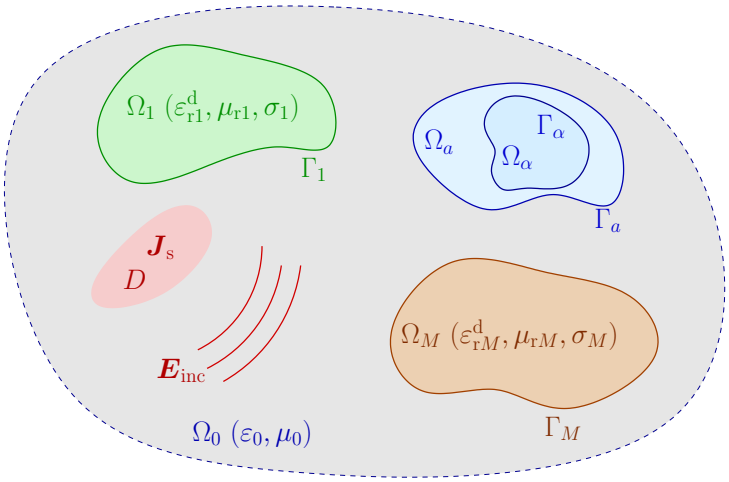

Figure 2. *Scattering by multiple objects, some of them bi-material: geometry and notation.*

Adequate rescaling of the additional terms will be determined by the leading order in η of the diagonal blocks $\boldsymbol{\mathcal{Z}}_\alpha^{\alpha\alpha} + \boldsymbol{\mathcal{Z}}_a^{\alpha\alpha}$ (which no longer involve the vacuum medium), easily found from (27a) to be

$$\boldsymbol{\mathcal{Z}}_\alpha^{\alpha\alpha} + \boldsymbol{\mathcal{Z}}_a^{\alpha\alpha} = O\left(\begin{bmatrix} 1 & 1 & 1 & 1 \\ 1 & \eta^{-2} & 1 & 1 \\ 1 & 1 & 1 & 1 \\ 1 & 1 & 1 & 1 \end{bmatrix}\right) \quad (a \in \mathcal{N}), \qquad \boldsymbol{\mathcal{Z}}_\alpha^{\alpha\alpha} + \boldsymbol{\mathcal{Z}}_a^{\alpha\alpha} = O\left(\begin{bmatrix} 1 & 1 & 1 & 1 \\ 1 & \eta^{-1} & 1 & 1 \\ 1 & 1 & 1 & 1 \\ 1 & 1 & 1 & 1 \end{bmatrix}\right) \quad (a \in \mathcal{M}).$$

Hence, no row scaling is required, while column scaling will depend on the surrounding medium D_a.

Non-conducting surrounding medium. For this case, we set

$$\boldsymbol{X}^\alpha = \boldsymbol{\Sigma}_\eta \widehat{\boldsymbol{X}}_\eta^\alpha, \quad \widehat{\boldsymbol{\mathcal{Z}}}_{\eta,a}^{\alpha\alpha} = \boldsymbol{\mathcal{Z}}_a^{\alpha\alpha}\boldsymbol{\Sigma}_\eta, \qquad \widehat{\boldsymbol{\mathcal{Z}}}_{\eta,\alpha}^{\alpha\alpha} = \boldsymbol{\mathcal{Z}}_\alpha^{\alpha\alpha}\boldsymbol{\Sigma}_\eta \qquad \text{with} \quad \boldsymbol{\Sigma}_\eta = \mathrm{Diag}\big[\boldsymbol{I},\, \eta^2\boldsymbol{I},\, \boldsymbol{I},\, \boldsymbol{I}\big]$$

and find the additional operator expansions

$$\widehat{\boldsymbol{\mathcal{Z}}}_{\eta,a}^{\alpha\alpha} = \widehat{\boldsymbol{\mathcal{Z}}}_{\mathrm{C}(0)}^{\alpha\alpha} + O(\eta^2), \qquad \widehat{\boldsymbol{\mathcal{Z}}}_{\eta,\alpha}^{\alpha\alpha} = \widehat{\boldsymbol{\mathcal{Z}}}_{\mathrm{N}(0)}^{\alpha\alpha} + O(\eta^2),$$

where $\widehat{\boldsymbol{\mathcal{Z}}}_{\mathrm{C}(0)}^{\alpha\alpha}$ is still given by (31), while $\widehat{\boldsymbol{\mathcal{Z}}}_{\mathrm{N}(0)}^{\alpha\alpha}$ must be derived anew due to the absence of row scaling and is given by (40) in Appendix A.2.

Moderately-conducting surrounding medium. For this case, we modify the column scaling and set

$$\boldsymbol{X}^\alpha = \boldsymbol{\Sigma}_\eta \widehat{\boldsymbol{X}}_\eta^\alpha, \quad \widehat{\boldsymbol{\mathcal{Z}}}_{\eta,a}^{\alpha\alpha} = \boldsymbol{\mathcal{Z}}_a^{\alpha\alpha}\boldsymbol{\Sigma}_\eta, \qquad \widehat{\boldsymbol{\mathcal{Z}}}_{\eta,\alpha}^{\alpha\alpha} = \boldsymbol{\mathcal{Z}}_\alpha^{\alpha\alpha}\boldsymbol{\Sigma}_\eta \qquad \text{with} \quad \boldsymbol{\Sigma}_\eta = \mathrm{Diag}\big[\boldsymbol{I},\, \eta\boldsymbol{I},\, \boldsymbol{I},\, \boldsymbol{I}\big]$$

and consequently find the additional operator expansions

$$\widehat{\boldsymbol{\mathcal{Z}}}_{\eta,a}^{\alpha\alpha} = \widehat{\boldsymbol{\mathcal{Z}}}_{\mathrm{C}(0)}^{\alpha\alpha} + \eta\widehat{\boldsymbol{\mathcal{Z}}}_{\mathrm{C}(1)}^{\alpha\alpha} + O(\eta^2), \qquad \widehat{\boldsymbol{\mathcal{Z}}}_{\eta,\alpha}^{\alpha\alpha} = \widehat{\boldsymbol{\mathcal{Z}}}_{\mathrm{M}(0)}^{\alpha\alpha} + \eta\widehat{\boldsymbol{\mathcal{Z}}}_{\mathrm{M}(1)}^{\alpha\alpha} + \eta^{3/2}\widehat{\boldsymbol{\mathcal{Z}}}_{\mathrm{M}(3/2)}^{\alpha\alpha} + O(\eta^2),$$

with $\widehat{\boldsymbol{\mathcal{Z}}}_{\mathrm{C}(0)}^{\alpha\alpha}$ still given by (31) while the other operator-valued coefficients must be rederived due to the absence of row scaling and are given in Appendix A.2 by (41) and (42).

Outcome. The foregoing considerations and the detailed formulas gathered in Appendix A.2 show that bi-material objects considered here generate, in expansions in powers of η of the relevant integral operator blocks, terms of the same orders as those arising from homogeneous objects with the medium type of their outer layer Ω_a. While the operator expansions (and thus the value of the asymptotic approximations of the current densities and related quantities) differ, the stage-1 part of the leading-order solution remains independent on the conductivity in Ω_a. Consequently, all results on approximation orders when NC or MC homogeneous bodies are present also apply to bi-material objects with the corresponding type of outer layer, including the validity at leading order of treating MC outer layers as NC.

3.4 Multiply-connected bodies. For a multiply-connected interface Γ_a, we have $\boldsymbol{\mathcal{V}}^a_{\rm L} = \mathbf{rot}_S H^{1/2}(\Gamma_a) \oplus \boldsymbol{\mathcal{V}}^a_{\rm G}$, where $\boldsymbol{\mathcal{V}}^a_{\rm G}$ is a finite-dimensional space of global loop functions [14]. Items b,c of Lemma 1 no longer apply when $\boldsymbol{\phi}_{\rm L} \in \boldsymbol{\mathcal{V}}^a_{\rm G}$; likewise, items d,e of Lemma 2 do not apply when both $\boldsymbol{\phi}^a_{\rm L}$ and $\boldsymbol{\phi}^b_{\rm L}$ are global loop functions. The additive decompositions of the unknown surface currents $\boldsymbol{J}^a, \boldsymbol{M}^a$ on a multiply-connected surface Γ_a are accordingly set as

$$\boldsymbol{J}^a = \boldsymbol{J}^a_{\rm L} + \boldsymbol{J}^a_{\rm G} + \boldsymbol{J}^a_{\rm T}, \qquad \boldsymbol{M}^a = \boldsymbol{M}^a_{\rm L} + \boldsymbol{M}^a_{\rm G} + \boldsymbol{M}^a_{\rm T},$$

with $\boldsymbol{J}^a_{\rm L}, \boldsymbol{M}^a_{\rm L} \in \mathbf{rot}_S H^{1/2}(\Gamma_a)$ and $\boldsymbol{J}^a_{\rm G}, \boldsymbol{M}^a_{\rm G} \in \boldsymbol{\mathcal{V}}^a_{\rm G}$. The asymptotic expansion of the PMCHWT integral problem presented in Section 2 can be adapted to the present case in a straightforward manner. For any body Ω_a for which Γ_a is multiply-connected, we set $\boldsymbol{X}^a = \{\boldsymbol{J}^a_{\rm L}, \boldsymbol{J}^a_{\rm G}, \boldsymbol{J}^a_{\rm T}, \boldsymbol{M}^a_{\rm L}, \boldsymbol{M}^a_{\rm G}, \boldsymbol{M}^a_{\rm T}\}^{\rm T}$ and decompose $\widetilde{\boldsymbol{X}}^a$ similarly. The rescaled operator matrices $\boldsymbol{\mathcal{Z}}^{ab}_{\ell}$ now have a 6×6 format, with the scaling applied to $\boldsymbol{J}^a_{\rm T}$ and $\widetilde{\boldsymbol{M}}^a_{\rm L}$ (i.e. third column and fourth row). We examine only the induced modifications on the leading-order approximation. The relevant 6×6 rescaled operator matrices $\widehat{\boldsymbol{\mathcal{Z}}}^{aa}_{(0)}$, $\widehat{\boldsymbol{\mathcal{Z}}}^{aa}_{\rm C(0)}$, $\widehat{\boldsymbol{\mathcal{Z}}}^{aa}_{\rm N(0)}$ and $\widehat{\boldsymbol{\mathcal{Z}}}^{aa}_{\rm M(0)}$, given in Appendix A.3, reveal that the global loop contributions $\boldsymbol{J}^a_{\rm G}, \boldsymbol{M}^a_{\rm G}$ to the surface current densities must be included in the unknowns of the stage-1 step of the leading-order system.

4 Numerical results.

In this section, we quantify the quality of the proposed asymptotic approximations by comparing their output values (surface current densities, impedance variation, internal or external electic and magnetic fields) to those from the full Maxwell PMCHWT problem. The latter is solved in rescaled form, using formulation (29) for homogeneous bodies or the rescaled version of formulation (39) discussed in Sec. 3.3 if bi-material interfaces are present, in order to alleviate low-frequency breakdown. We first demonstrate the main results of the foregoing asymptotic analysis on single-body and multiple-body configurations (Section 4.1), then apply our asymptotic approximation approach on EC testing cases (Section 4.2).

Each oriented closed surface Γ is modelled using a conforming mesh of triangular or quadrangular boundary elements, with each element edge shared by exactly two (adjacent) elements. Each element is non-degenerate, its unit normal being oriented consistently with the global orientation of Γ. For each mesh, the loop and tree subspaces are defined as linear combinations of usual $H_{\rm div}$ basis functions, known as RWG or rooftop functions for triangles and quadrilaterals, respectively. If Γ is multiply connected, the set of global loop basis functions is separated from the remaining (local) loop functions, as proposed in Section 3.4, in order to implement the matrix operator partitions given in Appendix A.3. Overall, these BE discretization methods are standard; we refer to e.g. [10] and [1] for details (see also [34] for an example of global loop functions on a cylinder). Element integrals are evaluated using Gauss-Legendre quadrature, with close interactions (characterized in terms of the distance of a quadrature point $\boldsymbol{q}_{\rm t}$ for the test integration to a trial element $e_{\rm b}$) regularized using polar coordinates in the parameter space of $e_{\rm b}$ about the projection of $\boldsymbol{q}_{\rm t}$ on $e_{\rm b}$. The matrix system is then solved using LU factorization applied either globally (for the rescaled PMCHWT matrix (17)) or blockwise (for the asymptotic model, see Sec. 2.6).

All results presented in this section were obtained using a in-house Matlab implementation of the foregoing BE discretization method for the PMCHWT system or its asymptotic approximation, run on a laptop computer with a 11th Gen Intel(R) Core(TM) i9-11950H@2.60 GHz processor. The symmetry and (where applicable) real-valuedness properties of operator blocks are not exploited at this proof-of-concept stage of the implementation, but should be in follow-up versions to be included in the simulation platform CIVA [12].

4.1 Validation examples. This first set of results aims at a direct numerical confirmation of the asymptotic approximations established in this work. Such assessments are done by examining relative differences between leading-order asymptotic approximations and their reference counterparts (evaluated using the rescaled full Maxwell PMCHWT formulation and indicated by a 'mxw' subscript where relevant). We consider first a single-body case, then a multi-body case that also activates extensions presented in Section 3. The proposed geometries and materials are chosen to be simple enough to be easily reproducible while avoiding trivial geometric invariances.

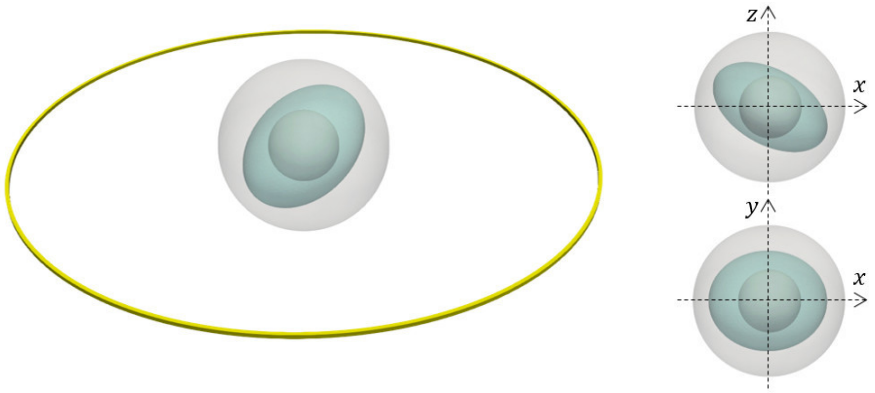

Figure 3. *Single-body example: sketch of the configuration showing the coil (left panel only), the ellipsoidal body (light blue), and the two spherical evaluation surfaces (grey).*

4.1.1 Single-body example. We consider a single body Ω_1 of ellipsoidal shape centered at the origin, with semiaxes (1, 0.8, 0.6) m and inclined (relative to the fixed frame $Oxyz$) by means of a 30° rotation about Oy. The BE mesh is created by deforming that of a unit sphere made of 4608 triangles. The source field is emitted by an annular coil (centered at O, with an internal radius of 4m and a square section of size 0.05 m) made of a single spire carrying a 1A current, so that the current density has magnitude $|\boldsymbol{J}_{\rm s}| = 400$ Am^{-2}. Resulting electric and magnetic fields are evaluated on the external sphere $S_0 \subset \Omega_0$ (center O, radius 1.2 m) and the internal sphere $S_1 \subset \Omega_1$ (center O, radius 0.4 m), each made of 12800 triangles (see Fig. 3). The characteristic length is set to $L = 1$ m. To estimate numerically the convergence rates of the asymptotic approximations provided by (36), (37a,b) and (38) as $\eta \to 0$, we compute Maxwell solutions and their leading-order asymptotic approximations for $\eta \in \left\{ 10^p,\, p = -6, -5, \ldots, 1 \right\}$ (setting the frequency $f = \omega/2\pi$ so that η defined by (20) takes the requisite values) and evaluate the relative differences between these quantities. The theoretical convergence rate for the latter is the order (relative to leading order) of the next term in the relevant asymptotic expansion.

We begin by setting the conductivity σ_1 as in (21) for the HC case (with $\xi_a = \sqrt{2}$), so that the object becomes highly conducting for small values of η, while $\mu_{\rm r1} = 10$. Some components of the electric and magnetic fields computed using the full asymptotic approximations (37a,b) with $\eta = 10^{-6}$ are plotted in Figure 4. The computed relative differences shown in Figure 5 are consistent with the relevant theoretical convergence rates, like in [6] where the proposed asymptotic approximation was limited to HC bodies.

By contrast, the present asymptotic formulation (with the conductivity classes defined by (20)) does not even require the presence of a HC body. Accordingly, we now take Ω_1 to be of either NC or MC type (with $\xi_a = 1$ in (21) for the MC case, and $\mu_{\rm r1} = 10$ for both cases). The computed relative differences shown in Figure 6 are again consistent with the relevant theoretical convergence rates, in particular reproducing the predicted loss of one order of convergence rate when Ω_1 is of MC type.

As discussed in Section 2.6, asymptotic approximations are computed using a two-stage approach if $\Omega_1 \in \mathcal{C}$ or $\mathcal{N}$ and a three-stage approach if $\Omega_1 \in \mathcal{M}$. Stage 1 alone provides the leading-order approximation of $\boldsymbol{H}$ and ΔZ, upon solving a system of size $3N/4$ ($\Omega_1 \in \mathcal{C}$) or $N/2$ ($\Omega_1 \in \mathcal{N}$ or $\mathcal{M}$). Moreover, in the latter two cases, those stage-1 systems are identical, while the achieved approximation orders are different (see Sec. 3.2), as corroborated by the results given in Table 1.

Finally, the removal of the static operator D_ℓ^{ab} in the double-layer potential occurring in loop-loop interactions (where it vanishes in the continuous PMCHWT formulation; see (26)) prevents the occurence of numerical noise on some components of the computed current densities, as illustrated in Figure 7 for the Maxwell problem on a Cartesian component of $\boldsymbol{M}$ whose pointwise magnitude is roughly half that of $\boldsymbol{M}$. Moreover, condition number values for the discretized integral operator matrix are stabilized (albeit still high), and close to those observed for the asymptotic approach, upon rescaling the Maxwell integral problem as indicated by the asymptotic approach, as shown in Table 2.

4.1.2 Multi-body example. We now consider a two-body example, as sketched in Figure 8, where in addition one of the bodies is bi-material with a multiply-connected embedded core. The source coil and

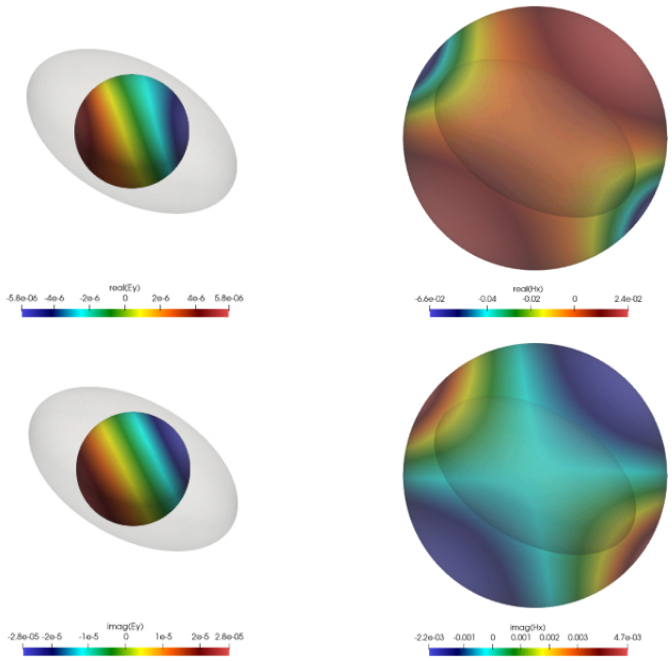

Figure 4. *Single-body example, HC body: real (top) and imaginary (bottom) parts of the internal electric (left) and external magnetic (right) fields for* $\eta = 10^{-6}$.

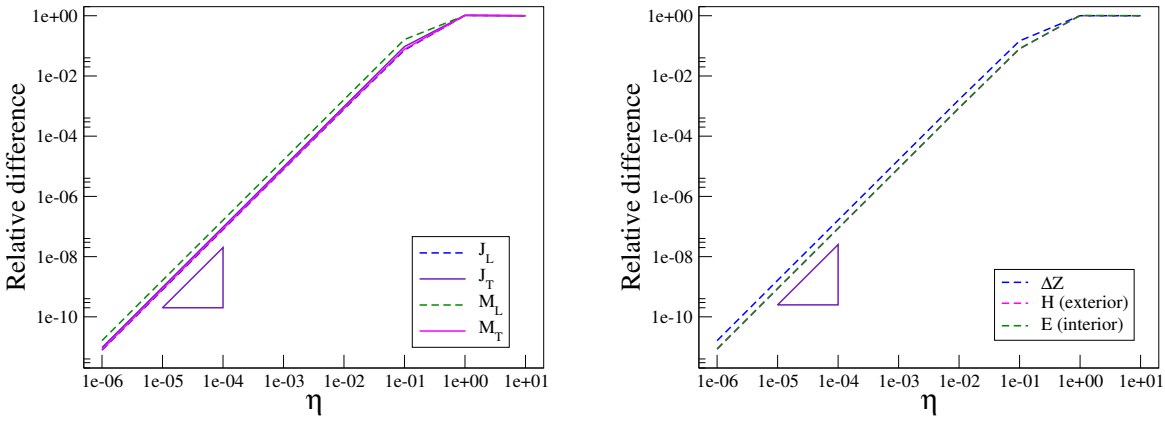

Figure 5. *Single-body example, HC body: convergence plots for the relative differences in the current densities (left) and the impedance variation and electromagnetic fields (right). Relative differences are defined as* $\|\boldsymbol{A} - \boldsymbol{A}_{mxw}\|/\|\boldsymbol{A}_{mxw}\|_{L^2(\Gamma)}$ *(for* $\boldsymbol{A} = \boldsymbol{J}_L, \boldsymbol{J}_T, \boldsymbol{M}_L, \boldsymbol{M}_T, \boldsymbol{H}, \boldsymbol{E}$*) or* $|\Delta Z - \Delta Z_{mxw}|/|\Delta Z_{mxw}|$*, where* $\boldsymbol{A}$ *or* ΔZ *is the leading-order approximations arising from* (36), (37a,b) *or* (38). *The triangles show* $O(\eta^2)$ *rates for visual comparison with theoretical orders of convergence.*

geometry of Ω_1 are as in Section 4.1.1. The configuration now comprises a second object Ω_2, of HC type and ellipsoidal shape; the domain Ω_2 is obtained by applying to a copy of Ω_1 a rotation of 120° about Oy and a translation of vector (2.0, −0.6, 0) m. In addition, a toroidal body $D_{\alpha(1)}$ is embedded inside Ω_1; that object is obtained by applying to a torus (created by rotating the circle centered at (0.3, 0, 0) m and of radius 0.1 m about the Oz axis) a deformation with ratios (1, 0.8, 0.6) and a 30° rotation about Ox. Both HC media correspond to $\xi_a = 1$ and $\mu_{ra} = 1$, the enveloping body to $\xi_a = 1$ (MC case) and $\mu_{ra} = 10$ (MC and NC). The BE meshes of Γ_1, Γ_2 are as that of Γ_1 in Section 4.1.1, while the mesh of the toroidal surface $\Gamma_{\alpha(1)}$, comprising 1 536 quadrilateral elements, is obtained by deforming a mesh of the generating torus.

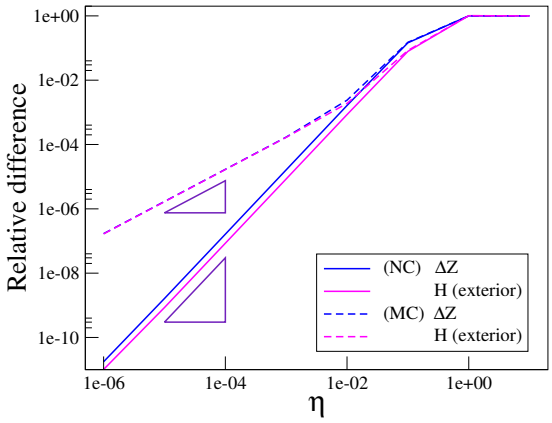

Figure 6. *Single-body example, NC or MC body: convergence plots for the relative differences in the impedance variation and external magnetic field. Relative differences are defined as* $\|\boldsymbol{H} - \boldsymbol{H}_{\text{mxw}}\|/\|\boldsymbol{H}_{\text{mxw}}\|_{L^2(\Gamma)}$ *and* $|\Delta Z - \Delta Z_{\text{mxw}}|/|\Delta Z_{\text{mxw}}|$*, where* $\boldsymbol{H}$ *and* ΔZ *are the leading-order approximations respectively arising from* (37b) *and* (38)*. The triangles show* $O(\eta)$ *and* $O(\eta^2)$ *rates for visual comparison with theoretical orders of convergence.*

η	ΔZ (HC)	D/η^2	ΔZ (MC)	D/η	ΔZ (NC)	D/η^2
10^{-1}	$3.4954\,10^{-1}+2.7912\,\mathrm{i}$	14.6	$1.6277\,10^{-1}+2.8287\,\mathrm{i}$	1.50	$1.1450\,10^{-1}+2.8317\,\mathrm{i}$	14.6
10^{-2}	$2.0226\,10^{-2}+2.4129\,10^{-1}\,\mathrm{i}$	16.3	$4.2352\,10^{-4}+2.4394\,10^{-1}\,\mathrm{i}$	.238	$1.0594\,10^{-5}+2.4394\,10^{-1}\,\mathrm{i}$	16.3
10^{-3}	$2.0181\,10^{-3}+2.4090\,10^{-2}\,\mathrm{i}$	16.3	$4.1233\,10^{-6}+2.4355\,10^{-2}\,\mathrm{i}$	.170	$1.0585\,10^{-9}+2.4355\,10^{-2}\,\mathrm{i}$	16.3
10^{-4}	$2.0181\,10^{-4}+2.4089\,10^{-3}\,\mathrm{i}$	16.3	$4.1222\,10^{-8}+2.4354\,10^{-3}\,\mathrm{i}$	.169	$1.0585\,10^{-13}+2.4354\,10^{-3}\,\mathrm{i}$	16.3
10^{-5}	$2.0181\,10^{-5}+2.4089\,10^{-4}\,\mathrm{i}$	16.3	$4.1222\,10^{-10}+2.4354\,10^{-4}\,\mathrm{i}$	.169	$1.0585\,10^{-17}+2.4354\,10^{-4}\,\mathrm{i}$	16.3
10^{-6}	$2.0181\,10^{-6}+2.4089\,10^{-5}\,\mathrm{i}$	16.2	$4.1222\,10^{-12}+2.4354\,10^{-5}\,\mathrm{i}$	.169	$1.0585\,10^{-21}+2.4354\,10^{-5}\,\mathrm{i}$	17.7

Table 1. *Single-body example: reference impedance variations and convergence of the relative differences* $D := |\Delta Z - \Delta Z_{\text{mxw}}|/|\Delta Z_{\text{mxw}}|$*, where* ΔZ *is the leading-order approximation arising from* (38)*.*

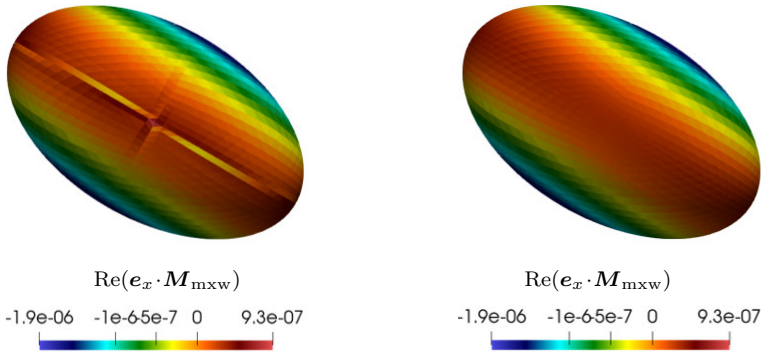

Figure 7. *Single-body example, HC object:* $Re(\boldsymbol{e}_x \cdot \boldsymbol{M}_{\text{mxw}})$ *in the* Oxz *plane (*$\boldsymbol{e}_x$*: Cartesian basis unit vector) for* $\eta = 10^{-6}$*, computed without (left) or with (right) suppression of the vanishing static double-layer operator* D_ℓ^{ab} *in the loop-loop interactions of the PMCHWT problem.*

This example hence activates options introduced in Section 2 (multiple disjoint bodies Ω_1, Ω_2), Section 3.3 (bi-material object $\Omega_1 = D_1 \cup D_{\alpha(1)}$) and Section 3.4 ($D_{\alpha(1)}$ is multiply-connected). Some components of the electric and magnetic fields computed using the full asymptotic approximations (37a,b) with $\eta = 10^{-6}$ are plotted in Figure 9. Here again, proceeding as explained in Section 4.1.1, the relative differences of all electromagnetic variables are found to verify the orders of convergence in η predicted by the analytic asymptotic expansions, see Figures 10 and 11. In particular, the presence of a MC object induces the loss of one unit in the convergence rates of all variables.

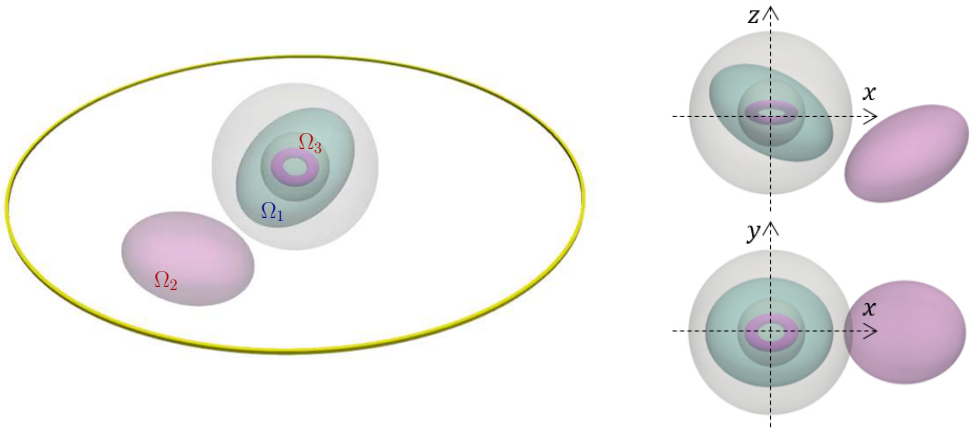

Figure 8. *Multi-body example: sketch of the configuration showing the coil (left panel only), the nonconductive or reasonably conductive ellipsoidal body, the disjointed ellipsoidal conductive body, the internal toroidal conductive body, and the two spherical evaluation surfaces.*

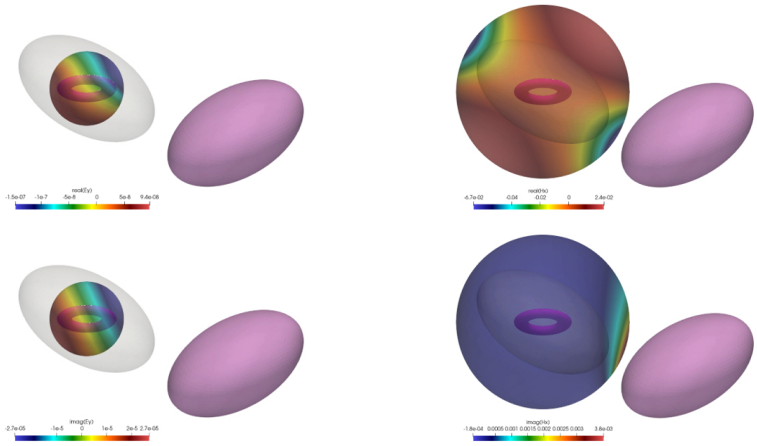

Figure 9. *Multi-body example: real (top) and imaginary (bottom) parts of the internal electric (right) and external magnetic (left) fields in the xy plane, for $\Omega_1 \in \mathcal{N}$ and $\eta = 10^{-6}$.*

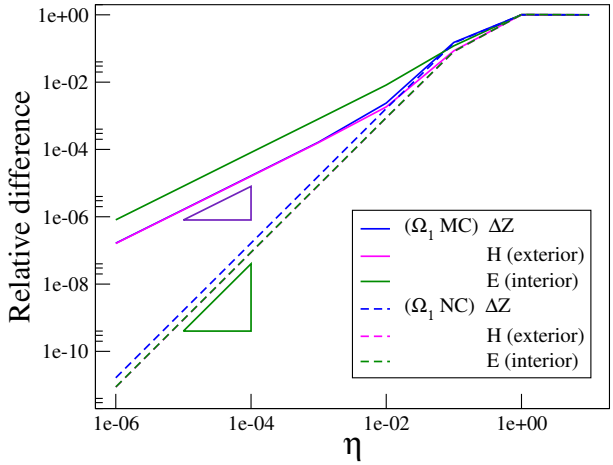

Figure 10. *Multi-body example: convergence of the relative differences $|\Delta Z - \Delta Z_{mxw}|/|\Delta Z_{mxw}|$, $\|\boldsymbol{H} - \boldsymbol{H}_{mxw}\|/\|\boldsymbol{H}_{mxw}\|_{L^2(S_0)}$ and $\|\boldsymbol{E} - \boldsymbol{E}_{mxw}\|/\|\boldsymbol{E}_{mxw}\|_{L^2(S_1)}$, where ΔZ, $\boldsymbol{H}$ and $\boldsymbol{E}$ are the leading-order approximations respectively arising from (38), (37b), (37a) and Ω_1 is either NC or MC.*

	PMCHWT	PMCHWT (rescaled)	Asymptotic
$\eta = 10^{-3}$	$1.1\,10^{14}$	$8.7\,10^{8}$	$8.6\,10^{8}$
$\eta = 10^{-6}$	$3.5\,10^{19}$	$8.7\,10^{8}$	$8.6\,10^{8}$

Table 2. *Single-body example, HC body: condition number of the governing linear system.*

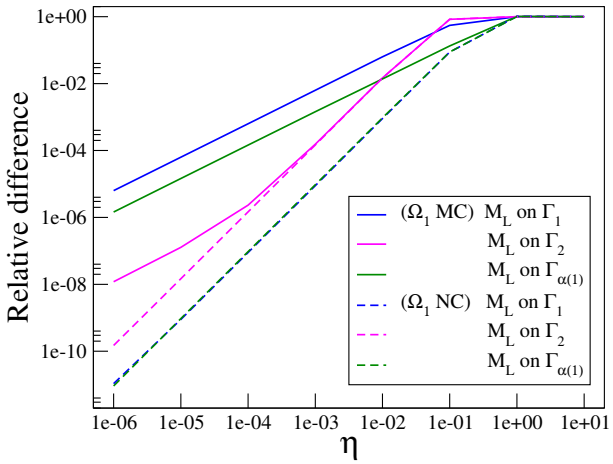

Figure 11. *Multi-body example: convergence of the relative differences* $\|\boldsymbol{M}_L - \boldsymbol{M}_{L,mxw}\|/\|\boldsymbol{M}_{L,mxw}\|_{L^2(\Gamma_a)}$ *on* Γ_1, Γ_2 *and* $\Gamma_{\alpha(1)}$, *where* $\boldsymbol{M}_L$ *is the leading-order approximations arising from* (36) *and* Ω_1 *is either NC or MC.*

4.2 Application to eddy current testing. Eddy current testing relies on the analysis of the impedance variation recorded at the terminals of a receiving coil. This variation reveals a perturbation in the circulation of eddy currents (ECs) $\sigma\boldsymbol{E}$, which are induced by an emitting coil carrying a prescribed current, in the HC medium under inspection. The penetration depth of ECs in a bulky metallic part is usually in a 0.1 mm to 10 mm range, with typical frequency ranges of 10 kHz to 1 MHz. This characteristic depth is set to the the skin depth: $L = \delta := \sqrt{2/\omega\sigma\mu}$. Eddy current testing allows to detect and characterize flaws such as corrosion or cracking, and also to assess geometrical or electromagnetic properties of some media (coating thickness, conductivity measurement).

The simulation of EC testing processes assists in the design, qualification or performance demonstration of an inspection process. In this regard, computational modelling is expected to reliably evaluate observable quantities such as the impedance variation, as well as the magnetic field in air for other processes not discussed here. Simulation also provides insight into the physics of EC testing, by quantifying other quantities not directly measured by the control apparatus, in particular the distribution of $\sigma\boldsymbol{E}$ in the inspected part and surrounding metallic objects. The estimation of perturbations of the magnetic field caused by nearby components is also needed in some instances, to evaluate the influence of nearby ferrite cores (whose magnetic permeability is non-neutral) or thick conducting parts used as magnetic shield in the sensor, in order to increase the magnetic field (and the induction) or reduce interferences between two coils, respectively. Coils are usually considered as sources immune from perturbation and modelled as volumic current loops $\boldsymbol{J}_{\rm s}$ in air satisfying the assumptions of Lemma 1. The impedance variation ΔZ is then found by a reciproicity argument to be given by (19).

In practice, the inspected part has known electromagnetic properties and the control experiment is calibrated to achieve a prescribed skin depth; this amounts to setting $\xi_a = \sqrt{2/\mu_{ra}}$ in (21) for a HC object.

4.2.1 TEAM 15 benchmark. In the TEAM #15 benchmark [26], to which a BE methodology is also applied in [5], a coil is moved along the axis of a pre-existing straight slot breaking the surface of a thick conducting plate (thickness $h = 12$ mm, conductivity $3.06\,10^7$ Sm^{-1}), see Figure 12. The main quantity of interest for this benchmark is the impedance variation $\Delta Z(x)$ at each coil position in the $0 \le x \le 30$ mm

	Asymptotic			Rescaled Maxwell			
	N	Assembly (s)	Solution (s)	N	Assembly (s)	Solution (s)	D
Mesh 1	7 645	54.8	2.2	10 260	68.2	4.5	$1.11\,10^{-2}$
Mesh 2	15 343	148.9	11.1	20 552	206.0	24.0	$6.15\,10^{-3}$
Mesh 3	39 107	910.7	122.3	52 294	1265.5	265.4	$2.58\,10^{-3}$

Table 3. *TEAM 15 benchmark: computational data for the three BE meshes used, N being the number of unknowns of the Stage-1 linear system of the asymptotic model (see Sec. 2.6), and of the full linear system for the rescaled Maxwell model (see Sec. 2.3). The quadratic mean relative differences D between ΔZ and ΔZ_{mxw} over all coil positions in the tube are also given.*

range, the slot being centered at the origin (coordinates (x, y, z) being as in Fig. 12). The configuration and measurement acquisition are comprehensively described in [27]. The control experiment is performed with a testing frequency of 7 kHz, resulting in a skin depth $\delta = 1.09$ mm.

As $\delta/h > 10$, the plate may reasonably be considered as being of infinite thickness for this experiment, so that BE meshes are limited to a large enough region of the upper plate surface $z = 0$, here taken as the rectangular region $(x, y) \in [-184, 214] \times [-184, 184]$ mm^2, and the slot itself. The BE analyses being made on an open surface, the edge DOFs on the outer edges are set to zero for a suitable definition of the $H_{\rm div}$ space and its Helmholtz-Hodge decomposition, the edge effects being in practice negligible. The region of interest on the plate surface is $(x, y) \in [-40, 70] \times [-40, 40]$ mm^2.

We denote thereafter by h_{xy} and h_z the element sizes in the (x, y) plane and along the slot depth direction z. The BE mesh near the slot is chosen to be fine enough that two elements fit along the slot thickness. Element sizes are gradually increased away from the slot, the sizes of two adjacent elements in the (x, y) plane being constrained to respect a ratio less than 2. We used three meshes, such that $(h_{xy}, h_z) = (4, 2)$, $(2, 1)$ or $(1, 0.5)$ mm for meshes 1 to 3, respectively, shown in Figure 13 together with the obtained surface current densities. The corresponding computed impedance variation $\Delta Z(x)$ is compared to the reference measurements in Figure 14. The simulation plots are calibrated using the measured values at $x = 29$ mm (which are themselves calibrated). Computational data for the simulation of complete scans is given in Table 3 and compared to the full, rescaled Maxwell simulation (for the present implementation and configurations, matrix assembly times are larger than solution times, although the latter grow more rapidly with the problem size, as expected). On this configuration, even mesh 1 achieves accuracy in ΔZ of the same order as experimental uncertainty despite the relatively coarse modeling of the slot region. Moreover, the results given for ΔZ by both methods are close, as shown in the last column, and increasingly so as the mesh is refined. Computations for the same benchmark in [5] use about $200,000$ scalar unknowns, and thus rely on BE compression techniques and an iterative solver.

Applications to other benchmarks typical of EC testing, done in e.g. [34] or [15] for benchmarks TEAM #7 et WFNDEC #15 respectively and then treated with a Maxwell formulation adapted to low-frequency regimes, elicited similar observations.

4.2.2 Inspection of a steam generator tube. Steam generator (SG) tubes in the pressurized water reactors (PWR) of nuclear power plants (NPPs) require periodic inspection. Each inspection entails scanning of thousands of 20 m-long bent tubes. Each tube is made of inconel (conductivity 1 MS m^{-1}, neutral relative permeability, thickness 1 mm, diameter 20 mm). Inspection frequencies are between 100 kHz and 600 kHz (inducing skin depths δ in the 1.5 to 0.5 mm range). Simulations of the EC testing process allows to assess the performance of various types of probes on critical cases involving tube cracking, signal alteration in the bent segment of the tube [16], and friction wear under antivibration bars (see e.g. [17, 31]) or under external deposits of weakly-conducting magnetic mud (which can accumulate as a dense, solid material in the flow slots between the tube and its support plate until clogging).

We model here the EC inspection of a moderately-bent SG tube ($\sigma_1 = 0.87$ MS m^{-1}, internal and external radii 8.435 mm and 9.525 mm, bending radius 200 mm) with a friction-wear flaw 0.4 mm deep. The tube may be additionally flawed by a slit (opening 50 μm, depth 40% of the tube thickness) breaking at the outer wall, an inox antivibration bar ($\sigma = 1.3$ MS/m) placed 100 μm away from the outer wall, or both (see Fig. 15). The probe is made of two axial coils operated in differential mode at 280 kHz, and

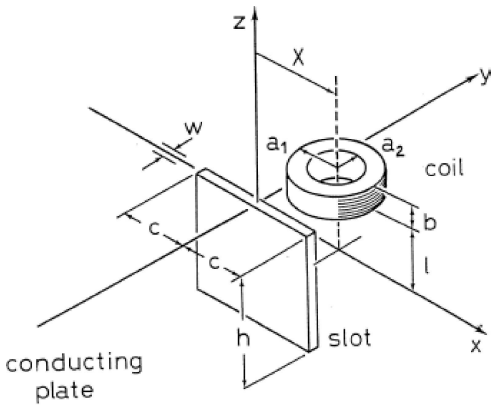

Figure 12. *TEAM 15 benchmark: configuration and notation (from* [27]*).*

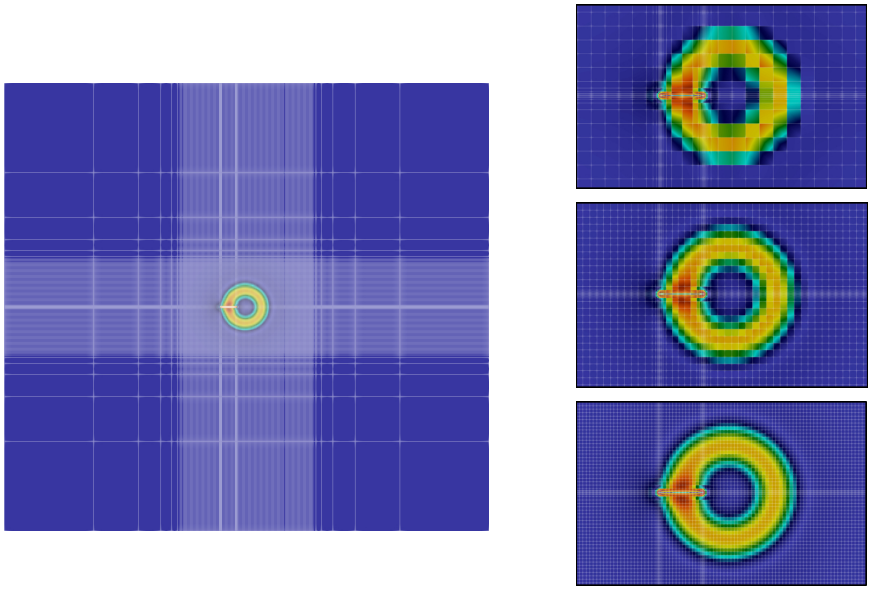

Figure 13. *TEAM 15 benchmark: mesh 3 and surface current density* $\mathrm{Im}(\boldsymbol{J}_s)$ *for the coil at* $x = 13.75$ *mm (left); close-ups of the slot region showing details of meshes 1 to 3 (right, top to bottom).*

the scan performed at positions between -25 mm et 25 mm spaced 0.25 mm apart along the tube axis, the central scan location corresponding to the flaw and the antivibration bar, if present (see Fig. 16).

The BE model features elements with a linear size of about 0.5 mm in the neighborhood of the flaw(s) and along the scan direction. As in the previous example, the mesh is gradually refined near the slit while made coarser away from the region of interest (with order-2 geometrical modeling used for accurate representation of edge and surface curvatures). Overall running times for complete scan simulations (including matrix set-up and factorization and all linear system solutions) are of about 40 min.

Acknowledgements.. The authors thank both reviewers for their careful reading of our paper and the useful remarks and suggestions offered.

References.

[1] Andriulli F.P. Loop-star and loop-tree decompositions: Analysis and efficient algorithms. *IEEE Trans. Antennas Propagat.*, **60**:2347–2356 (2012).

[2] Auld B.R., Muennemann F., Winslow D.K. Eddy current probe response to open and closed surface flaws. *J. Nondestr. Eval.* (1981).

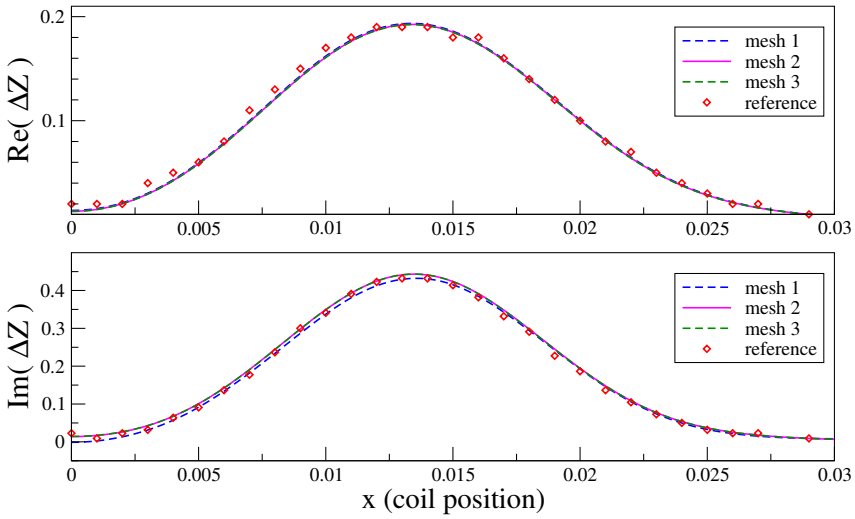

Figure 14. *TEAM 15 benchmark: real (top) and imaginary (bottom) parts of ΔZ against the coil position in the tube. The numerical results obtained with the three meshes of Fig. 13 are compared with reference measurements.*

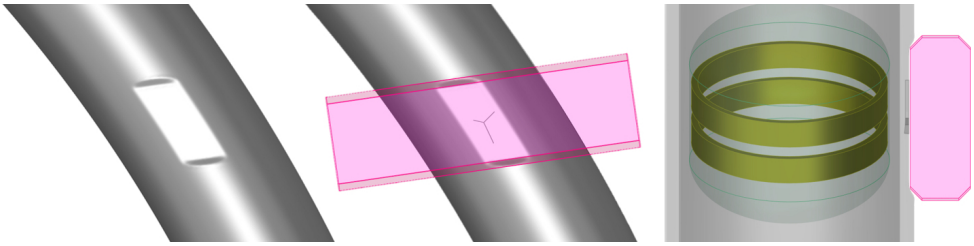

Figure 15. *SG tube: testing configuration. An axial probe made of two coils used in differential mode (shown in right image) moves along the tube axis. The anti-vibration bar (see center image) induces wear on the tube surface (see left image). In addition, a surface-breaking crack may appear (shown on center and right images).*

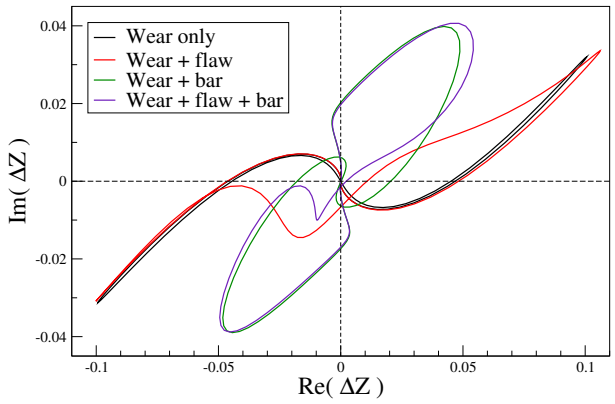

Figure 16. *SG tube: Values of the complex impedance variation ΔZ as the probe moves along the friction-worn tube, for the four considered situations.*

[3] Bao Y., Liu Z., Bowler J.R., Song J. Multilevel adaptive cross approximation for efficient modeling of 3D arbitrary shaped eddy current NDE problems. *NDT & E. Int.*, **104**:1–9 (2019).

[4] Bao Y., Song J. Analysis of electromagnetic non-destructive evaluation modelling using Stratton-Chu formulation-based fast algorithm. *Phil. Trans. Roy. Soc. A*, **378**:20190583 (2020).

[5] Bao Y., Wan T., Liu Z., Bowler J.R., Song J. Integral equation fast solver with truncated and degenerated kernel for computing flaw signals in eddy current non-destructive testing. *NDT & E. Int.*, **124**:102544 (2021).

[6] Bonnet M., Demaldent E. The eddy current model as a low-frequency, high-conductivity asymptotic form of the Maxwell transmission problem. *Comput. Math. Appl.*, **77**:2145–2161 (2019).

[7] Buffa A., Ciarlet Jr P. On traces for functional spaces related to Maxwell's equations. Part II: Hodge decompositions on the boundary of Lipschitz polyhedra and applications. *Math. Meth. in Appl. Sc.*, **24**:31–48 (2001).

[8] Buffa A., Costabel M., Sheen D. On traces for $H(\mathrm{curl}, \Omega)$ in Lipschitz domains. *J. Math. Anal. Appl.*, **276**:845–867 (2002).

[9] Buffa A., Hiptmair R., Von Petersdorff T., Schwab C. Boundary element methods for Maxwell transmission problems in Lipschitz domains. *Numer. Math.*, **95**:459–485 (2003).

[10] Chen S.Y., Chew W.C., Song J.M., Zhao J.S. Analysis of low frequency scattering from penetrable scatterers. *IEEE Trans. Geos. Remote Sens.*, **39**:726–735 (2001).

[11] Chhim T., Merlini A., Rahmouni L., Ortiz Guzman J.E., Andriulli F. Eddy current modeling in multiply connected regions via a full-wave solver based on the quasi-helmholtz projectors. *IEEE Open J. Antennas Propagat.*, **1**:534–548 (2020).

[12] CIVA, a multi-technique NDT simulation software platform developed by CEA. `https://www.extende.com` (2022).

[13] Colton D., Kress R. *Inverse acoustic and electromagnetic scattering theory*. Springer-Verlag (1998).

[14] Cools K.and Andriulli F.P., Olyslager F., Michielssen E. Nullspaces of MFIE and Calderón preconditioned EFIE operators applied to toroidal surfaces. *IEEE Trans. Antennas Propagat.*, **57** (2009).

[15] Demaldent E., Miorelli R., Reboud C., Theodoulidis T. Solution of the WFNDEC 2015 eddy current benchmark with surface integral equation method. In *AIP Conference Proceedings*, vol. 1706, page 190002 (2016).

[16] Demaldent E., Reboud C., Nozais F., Sollier T., Cattiaux G. Advances in modelling the ECT of U-bend steam generator tubes based on the boundary element method. In *Electromagnetic Non-Destructive Evaluation (XXI)*, Studies in Applied Electromagnetics and Mechanics, pages 167–174. IOS Press (2018).

[17] Demaldent E., Reboud C., Vigneron A., Nozais F., Boy J.B., Sollier T. Modelling of wear defects under an external object for the ECT of SG tubes. In *12th European Conference on Non-Destructive Testing* (2018).

[18] Hiptmair R. Boundary element methods for eddy current computation. In M. Schanz, O. Steinbach (editors), *Boundary Element Analysis*, vol. 29 of *Lecture Notes in Applied and Computational Mechanics*, pages 213–248. Springer-Verlag (2007).

[19] Homentcovschi D. Minimum-order regular boundary integral equations for three-dimensional eddy-current problem. *IEEEmag*, **38**:3433–3438 (2002).

[20] Ishibashi K. Eddy current analysis by BEM utilizing edge boundary condition. *IEEE Trans. Mag.*, **32**:832–835 (1996).

[21] Kalaichelvan S., Lavers J.D. Singularity evaluation in boundary integral equations of minimum order for 3-D eddy currents. *IEEE Trans. Mag.*, **5**:3053–3055 (1987).

[22] Kalaichelvan S., Lavers J.D. Boundary element methods for eddy current problems. In *Electromagnetic Applications*, pages 78–117. Springer (1989).

[23] Mayergoyz I. Boundary integral equations of minimum order for the calculation of three-dimensional eddy current problems. *IEEE Trans. Mag.*, **18**:536–539 (1982).

[24] Nédélec J.C. *Acoustic and electromagnetic equations: integral representations for harmonic problems*. Applied mathematical sciences (vol. 144). Springer (2001).

[25] Poggio A.J., Miller E.K. Integral Equation Solutions of Three-dimensional Scattering Problems. In R. Mittra (editor), *Computer Techniques for Electromagnetics (Chap. 4)*, International Series of Monographs in Electrical Engineering, pages 159 – 264. Pergamon (1973).

[26] Sabbagh H.A., Burke S.K. Benchmark problems in eddy-current NDE. In *Review of progress in quantitative nondestructive evaluation*, pages 217–224. Springer (1992).

[27] Sakellaris J.K., Prassianakis J., Tsamasphyros G., Shin Y.H., Seo H.Y. Verification of computational electromagnetic programs–the special case of team workshop problem 15 (rectangular slot in a thick plate): presentation of a problem in non destructive evaluation. 4th International Conference on NDT, Chania, Greece (2007).

[28] Schmindlin G., Fischer U., Andjelič Z., Schwab C. Preconditioning of the second-kind boundary integral equations for 3D eddy current problems. *Int. J. Numer. Meth. Engrg.*, **51**:1009–1031 (2001).

[29] Sharma S., Triverio P. Electromagnetic Modeling of Lossy Materials with a Potential-Based Boundary Element Method. *IEEE Antenn. Wirel. Propag. Lett.*, **21**:391–395 (2021).

[30] Smajic J., Andjelič Z., Bebendorf M. Fast BEM for eddy-current problems using H-matrices and adaptive cross approximation. *IEEE Trans. Mag.*, **43**:1269–1272 (2007).

[31] Sollier T., Decitre J.M., Vigneron A., Demaldent E. Simulation of eddy current testing of steam generator tubes with wear and secondary side magnetite deposits. *Insight*, **64** (2022, to appear).

[32] Todorov E.I. Measurement of electromagnetic properties of powder and solid metal materials for additive manufacturing. In *Nondestructive Characterization and Monitoring of Advanced Materials, Aerospace, and Civil Infrastructure 2017*, vol. 10169, page 1016907 (2017).

[33] Udpa S.S., Moore P.O. (editors). *Nondestructive testing handbook, third edition*. Amer. Soc. Nondestr. Testing (2004).

[34] Vigneron A., Demaldent E., Bonnet M. A multi-step solution algorithm for Maxwell boundary integral equations applied to low-frequency electromagnetic testing of conductive objects. *IEEE Trans. Mag.*, **52**:7005208 (2016).

[35] Yang M. *Efficient methods for solving boundary integral equation in diffusive scalar problem and eddy current nondestructive evaluation*. Ph.D. thesis, Iowa State University, USA (2010).

A Appendices.

A.1 Auxiliary proofs.

Proof of Lemma 1. Using that $\operatorname{div}(\boldsymbol{x}'\otimes\boldsymbol{J}_{\rm s}(\boldsymbol{x}')) = \boldsymbol{x}'\operatorname{div}\boldsymbol{J}_{\rm s} + \boldsymbol{J}_{\rm s}$ while G_1 is a constant function, we have

$$\boldsymbol{\Phi}_{(1)}[\boldsymbol{J}_{\rm s}](\boldsymbol{x}) = G_1\int_D \boldsymbol{J}_{\rm s}(\boldsymbol{x}')\,\mathrm{d}V(\boldsymbol{x}') = G_1\int_D \big(\operatorname{div}(\boldsymbol{x}'\otimes\boldsymbol{J}_{\rm s}(\boldsymbol{x}')) - \boldsymbol{x}'\operatorname{div}\boldsymbol{J}_{\rm s}\big)\,\mathrm{d}V(\boldsymbol{x}') = 0,$$

where the last equality results from the assumptions on $\boldsymbol{J}_{\rm s}$ and Green's identity. This proves (a).

Item (b) follows from integration by parts. Recall that $\boldsymbol{\mathcal{V}}^a_{\rm L} = \mathbf{rot}_S H^{1/2}(\Gamma_a) = \big\{\mathbf{rot}\,(\widetilde{\varphi}\boldsymbol{n})_{|\Gamma_a},\, \varphi\in H^{1/2}(\Gamma_a)\big\}$ (with $\widetilde{\varphi}$ denoting the extension of φ by a constant along the normal direction in a tubular neighborhood of Γ) for a simply-connected surface Γ_a. The vector potential $\boldsymbol{\Phi}_{(0)}[\boldsymbol{J}_{\rm s}]$ is harmonic outside of D, and hence satisfies $\mathbf{rot}\,\mathbf{rot}\,\boldsymbol{\Phi}_{(0)}[\boldsymbol{J}_{\rm s}] = \boldsymbol{\nabla}\operatorname{div}\boldsymbol{\Phi}_{(0)}[\boldsymbol{J}_{\rm s}] = 0$ (the last equality resulting from the assumptions on $\boldsymbol{J}_{\rm s}$), an integration by parts leads to (b).

Regarding item (c), using the expression (25) of H_3, we find

$$\mathbf{rot}\,\boldsymbol{\Phi}^{(3)}[\boldsymbol{J}_{\rm s}](\boldsymbol{x}) = -\frac{\mathrm{i}}{12\pi L^3}\int_D (\boldsymbol{x}-\boldsymbol{x}')\times\boldsymbol{J}_{\rm s}(\boldsymbol{x}')\,\mathrm{d}V(\boldsymbol{x}').$$

Now, using that $\boldsymbol{\phi}_{\rm L} = \mathbf{rot}\,(\widetilde{\varphi}\boldsymbol{n})_{|\Gamma_a}$ for some $\varphi\in H^{1/2}(\Gamma_a)$ since Γ_a is by assumption simply connected, we have

$$\begin{aligned}\int_{\Gamma_a}\boldsymbol{\phi}_{\rm L}(\boldsymbol{x})\cdot\big[(\boldsymbol{x}-\boldsymbol{x}')\times\boldsymbol{J}_{\rm s}(\boldsymbol{x}')\big]\,\mathrm{d}S(\boldsymbol{x}) &= \int_{\Gamma_a}\mathbf{rot}\,(\widetilde{\varphi}\boldsymbol{n})(\boldsymbol{x})\cdot\big[(\boldsymbol{x}-\boldsymbol{x}')\times\boldsymbol{J}_{\rm s}(\boldsymbol{x}')\big]\,\mathrm{d}S(\boldsymbol{x})\\ &= \int_{\Gamma_a}\widetilde{\varphi}\boldsymbol{n}(\boldsymbol{x})\cdot\mathbf{rot}\,\big((\boldsymbol{x}-\boldsymbol{x}')\times\boldsymbol{J}_{\rm s}(\boldsymbol{x}')\big)\mathrm{d}S(\boldsymbol{x}) = -2\int_{\Gamma_a}\widetilde{\varphi}\boldsymbol{n}(\boldsymbol{x})\cdot\boldsymbol{J}_{\rm s}(\boldsymbol{x}')\,\mathrm{d}S(\boldsymbol{x}).\end{aligned}$$

We therefore obtain (once more using the assumption $\boldsymbol{J}_{\rm s}\cdot\boldsymbol{n}=0$ on ∂D)

$$\big\langle\boldsymbol{\phi}_{\rm L},\,\boldsymbol{g}^a_{{\rm s}(3)}\big\rangle^a_\times = \frac{\mathrm{i}}{6\pi L^3}\int_{\Gamma_a}\widetilde{\varphi}\boldsymbol{n}\cdot\Big\{\int_D\boldsymbol{J}_{\rm s}\,\mathrm{d}V\Big\}\,\mathrm{d}S = \frac{\mathrm{i}}{6\pi L^3}\int_{\Gamma_a}\widetilde{\varphi}\boldsymbol{n}\cdot\Big\{\int_{\partial D}\boldsymbol{J}_{\rm s}\cdot\boldsymbol{n}\,\mathrm{d}S\Big\}\,\mathrm{d}S = 0.$$

Proof of Lemma 2. The proof of items (a) and (d) directly follows that of Lemma 1a,b. Item (b) stems from $H_1 = 0$, see expansions (24). Item (c) follows from item (a) by interchanging the trial and basis functions. Regarding item (e), assuming Γ_a to be simply connected and following the steps developed in the proof of Lemma 1c, we obtain

$$\big\langle\boldsymbol{\phi}^a_{\rm L},\,\boldsymbol{\mathcal{D}}^{ab}_{(3)}\boldsymbol{\phi}^b_{\rm L}\big\rangle^a_\times = \frac{\mathrm{i}}{6\pi L^3}\int_{\Gamma_a}\widetilde{\varphi}\boldsymbol{n}\cdot\Big\{\int_{\Gamma_b}\boldsymbol{\phi}^b_{\rm L}\,\mathrm{d}S\Big\}\,\mathrm{d}S = 0$$

since $\boldsymbol{\phi}^b_{\rm L}\in\boldsymbol{\mathcal{V}}^b_{\rm L}$. The case where Γ_b is simply connected while Γ_a is not follows by interchanging the trial and basis functions.

A.2 Operator expansions, bi-material object.

Additional operator-valued coefficient for a non-conducting surrounding medium:

$$\widehat{\boldsymbol{\mathcal{Z}}}^{\alpha\alpha}_{{\rm N}(0)} = \begin{bmatrix}\mu_{{\rm r}a}\mathbf{A}^{\alpha\alpha}_{(0)} & 0 & 0 & \mathbf{D}^{\alpha\alpha}_{(0)}\\ \mu_{{\rm r}a}\mathbf{A}^{\alpha\alpha}_{(0)} & \mu_{{\rm r}a}q_a^{-2}\mathbf{K}^{\alpha\alpha}_{(0)} & \mathbf{D}^{\alpha\alpha}_{(0)} & \mathbf{D}^{\alpha\alpha}_{(0)}\\ 0 & 0 & 0 & 0\\ \mathbf{D}^{\alpha\alpha}_{(0)} & 0 & 0 & \mu_{{\rm r}a}^{-1}\mathbf{K}^{\alpha\alpha}_{(0)}\end{bmatrix}. \tag{40}$$

Additional operator-valued coefficients for a moderately-conducting surrounding medium:

$$\widehat{\boldsymbol{\mathcal{Z}}}^{\alpha\alpha}_{{\rm C}(1)} = \begin{bmatrix}0 & \mu_{{\rm r}a}\mathbf{A}^{aa}_{{\rm C}(0)} & 0 & 0\\ 0 & \mu_{{\rm r}a}(\mathbf{A}^{aa}_{{\rm C}(0)} + q_a^{-2}\mathbf{K}^{aa}_{{\rm C}(0)}) & 0 & 0\\ 0 & \mathbf{D}^{aa}_{{\rm C}(0)} & 0 & 0\\ 0 & \mathbf{D}^{aa}_{{\rm C}(0)} & 0 & 0\end{bmatrix} \tag{41}$$

and

$$
\widehat{\mathcal{Z}}^{\alpha\alpha}_{\mathrm{M}(0)} = \begin{bmatrix} \mu_{\mathrm{r}\alpha}\mathbf{A}^{\alpha\alpha}_{(0)} & 0 & 0 & \mathbf{D}^{\alpha\alpha}_{(0)} \\ \mu_{\mathrm{r}\alpha}\mathbf{A}^{\alpha\alpha}_{(0)} & \mu_{\mathrm{r}\alpha}q_\alpha^{-2}\mathbf{K}^{\alpha\alpha}_{(0)} & \mathbf{D}^{\alpha\alpha}_{(0)} & \mathbf{D}^{\alpha\alpha}_{(0)} \\ 0 & 0 & 0 & 0 \\ \mathbf{D}^{\alpha\alpha}_{(0)} & 0 & 0 & \mu_{\mathrm{r}\alpha}^{-1}\mathbf{K}^{\alpha\alpha}_{(0)} \end{bmatrix},
$$

$$
\widehat{\mathcal{Z}}^{\alpha\alpha}_{\mathrm{M}(1)} = \begin{bmatrix} \mu_{\mathrm{r}\alpha}q_\alpha^2\mathbf{A}^{\alpha\alpha}_{(2)} & \mu_{\mathrm{r}\alpha}\mathbf{A}^{\alpha\alpha}_{(0)} & q_\alpha^2\mathbf{D}^{\alpha\alpha}_{(2)} & q_\alpha^2\mathbf{D}^{\alpha\alpha}_{(2)} \\ \mu_{\mathrm{r}\alpha}q_\alpha^2\mathbf{A}^{\alpha\alpha}_{(2)} & \mu_{\mathrm{r}\alpha}(\mathbf{A}^{\alpha\alpha}_{(0)} - 2q'_\alpha\mathbf{K}^{\alpha\alpha}_{(0)} + \mathbf{K}^{\alpha\alpha}_{(2)}) & q_\alpha^2\mathbf{D}^{\alpha\alpha}_{(2)} & q_\alpha^2\mathbf{D}^{\alpha\alpha}_{(2)} \\ q_\alpha^2\mathbf{D}^{\alpha\alpha}_{(2)} & \mathbf{D}^{\alpha\alpha}_{(0)} & \mu_{\mathrm{r}\alpha}^{-1}q_\alpha^2\mathbf{A}^{\alpha\alpha}_{(0)} & \mu_{\mathrm{r}\alpha}^{-1}q_\alpha^2\mathbf{A}^{\alpha\alpha}_{(0)} \\ q_\alpha^2\mathbf{D}^{\alpha\alpha}_{(2)} & \mathbf{D}^{\alpha\alpha}_{(0)} & \mu_{\mathrm{r}\alpha}^{-1}q_\alpha^2\mathbf{A}^{\alpha\alpha}_{(0)} & \mu_{\mathrm{r}\alpha}^{-1}q_\alpha^2(\mathbf{A}^{\alpha\alpha}_{(0)} + \mathbf{K}^{\alpha\alpha}_{(2)}) \end{bmatrix}, \tag{42}
$$

$$
\widehat{\mathcal{Z}}^{\alpha\alpha}_{\mathrm{M}(3/2)} = \begin{bmatrix} \mu_{\mathrm{r}\alpha}q_\alpha^3\mathbf{A}^{\alpha\alpha}_{(3)} & 0 & 0 & q_\alpha^3\mathbf{D}^{\alpha\alpha}_{(3)} \\ \mu_{\mathrm{r}\alpha}q_\alpha^3\mathbf{A}^{\alpha\alpha}_{(3)} & \mu_{\mathrm{r}\alpha}q_\alpha\mathbf{A}^{\alpha\alpha}_{(1)} & q_\alpha^3\mathbf{D}^{\alpha\alpha}_{(3)} & q_\alpha^3\mathbf{D}^{\alpha\alpha}_{(3)} \\ 0 & 0 & 0 & 0 \\ q_\alpha^3\mathbf{D}^{\alpha\alpha}_{(3)} & 0 & 0 & \mu_{\mathrm{r}\alpha}^{-1}q_\alpha^3(\mathbf{A}^{\alpha\alpha}_{(1)} + \mathbf{K}^{\alpha\alpha}_{(3)}) \end{bmatrix}
$$

A.3 Operator expansions, multiply-connected object. The leading-order operator matrices $\widehat{\mathcal{Z}}^{ab}_{(0)}$ for the vacuum medium are found to be given by

$$
\widehat{\mathcal{Z}}^{ab}_{(0)} = \begin{bmatrix} \mathbf{A}^{ab}_{(0)} & \mathbf{A}^{ab}_{(0)} & 0 & 0 & 0 & \mathbf{D}^{ab}_{(0)} \\ \mathbf{A}^{ab}_{(0)} & \mathbf{A}^{ab}_{(0)} & 0 & 0 & \mathbf{D}^{ab}_{(0)} & \mathbf{D}^{ab}_{(0)} \\ \mathbf{A}^{ab}_{(0)} & \mathbf{A}^{ab}_{(0)} & \mathbf{K}^{ab}_{(0)} & \mathbf{D}^{ab}_{(0)} & \mathbf{D}^{ab}_{(0)} & \mathbf{D}^{ab}_{(0)} \\ 0 & 0 & 0 & 0 & 0 & 0 \\ 0 & \mathbf{D}^{ab}_{(0)} & 0 & 0 & 0 & 0 \\ \mathbf{D}^{ab}_{(0)} & \mathbf{D}^{ab}_{(0)} & 0 & 0 & 0 & \mathbf{K}^{ab}_{(0)} \end{bmatrix} \qquad (a \in \mathcal{C} \cup \mathcal{M}),
$$

$$
= \begin{bmatrix} \mathbf{A}^{ab}_{(0)} & \mathbf{A}^{ab}_{(0)} & 0 & 0 & 0 & \mathbf{D}^{ab}_{(0)} \\ \mathbf{A}^{ab}_{(0)} & \mathbf{A}^{ab}_{(0)} & 0 & 0 & \mathbf{D}^{ab}_{(0)} & \mathbf{D}^{ab}_{(0)} \\ \mathbf{A}^{ab}_{(0)} & \mathbf{A}^{ab}_{(0)} & \mathbf{K}^{ab}_{(0)} & \mathbf{D}^{ab}_{(0)} & \mathbf{D}^{ab}_{(0)} & \mathbf{D}^{ab}_{(0)} \\ \mathbf{D}^{ab}_{(2)} & \mathbf{D}^{ab}_{(2)} & \mathbf{D}^{ab}_{(0)} & \mathbf{A}^{ab}_{(0)} & \mathbf{A}^{ab}_{(0)} & \mathbf{A}^{ab}_{(0)} \\ 0 & \mathbf{D}^{ab}_{(0)} & 0 & 0 & 0 & 0 \\ \mathbf{D}^{ab}_{(0)} & \mathbf{D}^{ab}_{(0)} & 0 & 0 & 0 & \mathbf{K}^{ab}_{(0)} \end{bmatrix} \qquad (a \in \mathcal{N}),
$$

while those for the three types of media considered for the scattering objects are found as

$$
\widehat{\mathcal{Z}}^{aa}_{\mathrm{C}(0)} = \begin{bmatrix} \mu_{\mathrm{r}a}\mathbf{A}^{aa}_{\mathrm{C}(0)} & \mu_{\mathrm{r}a}\mathbf{A}^{aa}_{\mathrm{C}(0)} & 0 & \mathbf{D}^{aa}_{\mathrm{C}(0)} & \mathbf{D}^{aa}_{\mathrm{C}(0)} & \mathbf{D}^{aa}_{\mathrm{C}(0)} \\ \mu_{\mathrm{r}a}\mathbf{A}^{aa}_{\mathrm{C}(0)} & \mu_{\mathrm{r}a}\mathbf{A}^{aa}_{\mathrm{C}(0)} & 0 & \mathbf{D}^{aa}_{\mathrm{C}(0)} & \mathbf{D}^{aa}_{\mathrm{C}(0)} & \mathbf{D}^{aa}_{\mathrm{C}(0)} \\ \mu_{\mathrm{r}a}\mathbf{A}^{aa}_{\mathrm{C}(0)} & \mu_{\mathrm{r}a}\mathbf{A}^{aa}_{\mathrm{C}(0)} & 0 & \mathbf{D}^{aa}_{\mathrm{C}(0)} & \mathbf{D}^{aa}_{\mathrm{C}(0)} & \mathbf{D}^{aa}_{\mathrm{C}(0)} \\ \mathbf{D}^{aa}_{\mathrm{C}(0)} & \mathbf{D}^{aa}_{\mathrm{C}(0)} & 0 & \mu_{\mathrm{r}a}^{-1}q_a^2\mathbf{A}^{aa}_{\mathrm{C}(0)} & \mu_{\mathrm{r}a}^{-1}q_a^2\mathbf{A}^{aa}_{\mathrm{C}(0)} & \mu_{\mathrm{r}a}^{-1}q_a^2\mathbf{A}^{aa}_{\mathrm{C}(0)} \\ \mathbf{D}^{aa}_{\mathrm{C}(0)} & \mathbf{D}^{aa}_{\mathrm{C}(0)} & 0 & \mu_{\mathrm{r}a}^{-1}q_a^2\mathbf{A}^{aa}_{\mathrm{C}(0)} & \mu_{\mathrm{r}a}^{-1}q_a^2\mathbf{A}^{aa}_{\mathrm{C}(0)} & \mu_{\mathrm{r}a}^{-1}q_a^2\mathbf{A}^{aa}_{\mathrm{C}(0)} \\ \mathbf{D}^{aa}_{\mathrm{C}(0)} & \mathbf{D}^{aa}_{\mathrm{C}(0)} & 0 & \mu_{\mathrm{r}a}^{-1}q_a^2\mathbf{A}^{aa}_{\mathrm{C}(0)} & \mu_{\mathrm{r}a}^{-1}q_a^2\mathbf{A}^{aa}_{\mathrm{C}(0)} & \mu_{\mathrm{r}a}^{-1}(q_a^2\mathbf{A}^{aa}_{\mathrm{C}(0)} + \mathbf{K}^{aa}_{\mathrm{C}(0)}) \end{bmatrix},
$$

$$
\widehat{\mathcal{Z}}^{aa}_{\mathrm{N}(0)} = \begin{bmatrix} \mu_{\mathrm{r}a}\mathbf{A}^{aa}_{(0)} & \mu_{\mathrm{r}a}\mathbf{A}^{aa}_{(0)} & 0 & 0 & 0 & \mathbf{D}^{aa}_{(0)} \\ \mu_{\mathrm{r}a}\mathbf{A}^{aa}_{(0)} & \mu_{\mathrm{r}a}\mathbf{A}^{aa}_{(0)} & 0 & 0 & \mathbf{D}^{aa}_{(0)} & \mathbf{D}^{aa}_{(0)} \\ \mu_{\mathrm{r}a}\mathbf{A}^{aa}_{(0)} & \mu_{\mathrm{r}a}\mathbf{A}^{aa}_{(0)} & \mu_{\mathrm{r}a}q_a^{-2}\mathbf{K}^{aa}_{(0)} & \mathbf{D}^{aa}_{(0)} & \mathbf{D}^{aa}_{(0)} & \mathbf{D}^{aa}_{(0)} \\ q_a^2\mathbf{D}^{aa}_{(2)} & q_a^2\mathbf{D}^{aa}_{(2)} & \mathbf{D}^{aa}_{(0)} & \mu_{\mathrm{r}a}^{-1}q_a^2\mathbf{A}^{aa}_{(0)} & \mu_{\mathrm{r}a}^{-1}q_a^2\mathbf{A}^{aa}_{(0)} & \mu_{\mathrm{r}a}^{-1}q_a^2\mathbf{A}^{aa}_{(0)} \\ 0 & \mathbf{D}^{aa}_{(0)} & 0 & 0 & 0 & 0 \\ \mathbf{D}^{aa}_{(0)} & \mathbf{D}^{aa}_{(0)} & 0 & 0 & 0 & \mu_{\mathrm{r}a}^{-1}\mathbf{K}^{aa}_{(0)} \end{bmatrix},
$$

$$
\widehat{\mathcal{Z}}^{aa}_{\mathrm{M}(0)} = \begin{bmatrix} \mu_{\mathrm{r}a}\mathbf{A}^{aa}_{(0)} & \mu_{\mathrm{r}a}\mathbf{A}^{aa}_{(0)} & 0 & 0 & 0 & \mathbf{D}^{aa}_{(0)} \\ \mu_{\mathrm{r}a}\mathbf{A}^{aa}_{(0)} & \mu_{\mathrm{r}a}\mathbf{A}^{aa}_{(0)} & 0 & 0 & \mathbf{D}^{aa}_{(0)} & \mathbf{D}^{aa}_{(0)} \\ \mu_{\mathrm{r}a}\mathbf{A}^{aa}_{(0)} & \mu_{\mathrm{r}a}\mathbf{A}^{aa}_{(0)} & 0 & \mathbf{D}^{aa}_{(0)} & \mathbf{D}^{aa}_{(0)} & \mathbf{D}^{aa}_{(0)} \\ q_a^2\mathbf{D}^{aa}_{(2)} & q_a^2\mathbf{D}^{aa}_{(2)} & 0 & \mu_{\mathrm{r}a}^{-1}q_a^2\mathbf{A}^{aa}_{(0)} & \mu_{\mathrm{r}a}^{-1}q_a^2\mathbf{A}^{aa}_{(0)} & \mu_{\mathrm{r}a}^{-1}q_a^2\mathbf{A}^{aa}_{(0)} \\ 0 & \mathbf{D}^{aa}_{(0)} & 0 & 0 & 0 & \mu_{\mathrm{r}a}^{-1}\mathbf{K}^{aa}_{(0)} \\ \mathbf{D}^{aa}_{(0)} & \mathbf{D}^{aa}_{(0)} & 0 & 0 & 0 & \mu_{\mathrm{r}a}^{-1}\mathbf{K}^{aa}_{(0)} \end{bmatrix}.
$$